

RESEARCH ARTICLE

# Isolating and quantifying the role of developmental noise in generating phenotypic variation

Maria Kiskowski<sup>1\*</sup>, Tilmann Glimm<sup>2</sup>, Nickolas Moreno<sup>3</sup>, Tony Gamble<sup>4,5,6</sup>, Ylenia Chiari<sup>3,7</sup>

**1** University of South Alabama, Department of Mathematics and Statistics, Mobile, AL, United States of America, **2** Western Washington University, Department of Mathematics, Bellingham, WA, United States of America, **3** University of South Alabama, Department of Biology, Mobile, AL, United States of America, **4** Department of Biological Sciences, Marquette University, Milwaukee, WI, United States of America, **5** Bell Museum of Natural History, University of Minnesota, St. Paul, MN, United States of America, **6** Milwaukee Public Museum, Milwaukee, WI, United States of America, **7** George Mason University, Department of Biology, Science & Technology Campus, Manassas, VA, United States of America

\* [abyrne@southalabama.edu](mailto:abyrne@southalabama.edu)



**OPEN ACCESS**

**Citation:** Kiskowski M, Glimm T, Moreno N, Gamble T, Chiari Y (2019) Isolating and quantifying the role of developmental noise in generating phenotypic variation. *PLoS Comput Biol* 15(4): e1006943. <https://doi.org/10.1371/journal.pcbi.1006943>

**Editor:** Philip K. Maini, Oxford, UNITED KINGDOM

**Received:** July 4, 2018

**Accepted:** March 11, 2019

**Published:** April 22, 2019

**Copyright:** © 2019 Kiskowski et al. This is an open access article distributed under the terms of the [Creative Commons Attribution License](https://creativecommons.org/licenses/by/4.0/), which permits unrestricted use, distribution, and reproduction in any medium, provided the original author and source are credited.

**Data Availability Statement:** Original and processed gecko images, and matlab scripts generating figures, will be available for download at [github.com/geckodevnoise/pcompbio2019](https://github.com/geckodevnoise/pcompbio2019), a persistent GitHub repository.

**Funding:** Funding was provided by the Gulf Coast Advance Fellowship (<http://www.gulfcoastadvance.org/home-2-1/>) and USA Research and Development Fund (<http://www.southalabama.edu/departments/research/rd/funding-opportunities/internal-funding-opportunities.html>) to YC. The funders had no role in study design, data collection

## Abstract

Genotypic variation, environmental variation, and their interaction may produce variation in the developmental process and cause phenotypic differences among individuals. Developmental noise, which arises during development from stochasticity in cellular and molecular processes when genotype and environment are fixed, also contributes to phenotypic variation. While evolutionary biology has long focused on teasing apart the relative contribution of genes and environment to phenotypic variation, our understanding of the role of developmental noise has lagged due to technical difficulties in directly measuring the contribution of developmental noise. The influence of developmental noise is likely underestimated in studies of phenotypic variation due to intrinsic mechanisms within organisms that stabilize phenotypes and decrease variation. Since we are just beginning to appreciate the extent to which phenotypic variation due to stochasticity is potentially adaptive, the contribution of developmental noise to phenotypic variation must be separated and measured to fully understand its role in evolution. Here, we show that variation in the component of the developmental process corresponding to environmental and genetic factors (here treated together as a unit called the LALI-type) versus the contribution of developmental noise, can be distinguished for leopard gecko (*Eublepharis macularius*) head color patterns using mathematical simulations that model the role of random variation (corresponding to developmental noise) in patterning. Specifically, we modified the parameters of simulations corresponding to variation in the LALI-type to generate the full range of phenotypic variation in color pattern seen on the heads of eight leopard geckos. We observed that over the range of these parameters, variation in color pattern due to LALI-type variation exceeds that due to developmental noise in the studied gecko cohort. However, the effect of developmental noise on patterning is also substantial. Our approach addresses one of the major goals of evolutionary biology: to quantify the role of stochasticity in shaping phenotypic variation.

and analysis, decision to publish, or preparation of the manuscript.

**Competing interests:** The authors have declared that no competing interests exist.

## Author summary

The observable characteristics of an organism make up its phenotype. Variation among phenotypes is due to genetic differences, environmental factors and developmental noise (effects due to inherent stochasticity) during development. We used mathematical models to investigate the contributions of variation of the developmental process due to genetic and environmental factors (treated in this work as a single unit) versus developmental noise (unavoidable variation within the developmental program) to the development of pigment patterns on gecko heads. We found that for our cohort, the proportion of phenotypic variation due to variation in the unit composed of genotypic and environmental variation is larger than that due to developmental noise. Furthermore, by allowing the parameters of the mathematical model to vary, we generated the full extent of potential phenotypic pattern variation that could occur on the head of geckos. This serves to further study the influence of the buffering mechanisms (canalization, selection, and developmental stability) limiting phenotypic variation. This approach can be applied to any regular morphological trait that results from self-organized processes such as reaction-diffusion mechanisms, including the frequently found striped and spotted patterns of animal pigmentation patterning, patterning of bones in vertebrate limbs, and body segmentation in segmented animals.

## Introduction

A first-order approximation of phenotypic variation is that genotype and environment variation maps to phenotype variation. Stochastic variation is an important third source of phenotype variation included in a more complete description of the genotype-phenotype mapping [1–4]. Therefore, at the developmental level, genotypic (developmental program) and/or environmental changes, or stochastic variation can generate developmental variation. This stochastic variation, called *developmental noise*, is the difference in phenotypic outcomes that occurs when genotype and environment are fixed (e.g., [5–7]), due to stochasticity in cellular and molecular processes [4, 6]. The interaction of these sources of variation (genotype, environment, and stochasticity), combined with the sheer magnitude of the number of phenotypic variables, makes the study of the phenotypic variation of a population extremely complex.

Computational morphometric approaches may identify a small number of key phenotype features (comparable “units” [8]) or apply clustering analyses over a higher number of phenotype variables, to objectively sort complex phenotypic variations and quantify differences between them. Here we describe a different computational approach for interpreting phenotypic differences among individuals at the same selected developmental time. We describe phenotypic variation in the context of the relative contribution of components of the developmental process, that in this work are treated together as a unit (genotype and environment), and developmental noise. In our stochastic simulations, non-stochastic (predetermined) parameters correspond to genetic and environmental factors considered together as a unit called the LALI-type (see below and Table 1) while stochastic variation within simulations corresponds to development noise. By applying a computational model of a developmental mechanism to generate phenotypes, such as the reaction diffusion model we use here, the simulated phenotype variation will reflect the intrinsic freedoms and constraints of the developmental mechanism itself [9, 10]. While various methods are commonly used to discern the relative contribution of genotype versus environment in shaping phenotypic variation (e.g.,

controlled captive breeding approaches, QTL, and quantitative genetics), being able to isolate and quantify the importance of developmental noise on such a phenotypic variation is currently still very challenging. The potential influence of developmental noise is likely underestimated in studies of phenotypic variation due to intrinsic mechanisms within organisms that stabilize phenotypes and decrease variation (for example, in estimates of developmental noise based on fluctuating asymmetries [11]). In this work, we therefore do not analyze each component (genotype, environment, developmental noise) of the developmental process alone, but we use different fixed combinations of genotype and environment taken together (each one of them called LALI-type, see below and Table 1) versus developmental noise to estimate the influence of variation in LALI-type and developmental noise on phenotypic variation.

Patterns that are self-organized are characterized by significant pattern variation that is due to random factors even when genetic and environmental patterning parameters are held fixed. The methodology described here can be used to measure the extent of random variation that is due to the random component of such a mechanism, providing a lower bound for variation inherent to the mechanism that is useful for interpreting the total variation that is observed. Further, a sensitivity analysis of the effect of varying genetic and environmental pattern parameters provides a framework for the topology of this variation, as it can be understood which ranges of parameters map to different ranges of phenotypes. The method can be applied to individual phenotypes, one at a time, without requiring a population distribution of the variation, as we have done here, to predict the variation of clones under identical environmental and genetic conditions or determine the probability that two phenotypes could result under identical environmental and genetic conditions. While our methodology to measure the role of noise on the variation is applicable to any

**Table 1. Definitions of the terms used in this manuscript relating to the L→P map.**

LALI mechanism	A LALI mechanism is a mechanism for periodic patterning based on local activation and long range inhibition (LALI; [23–25]).
LALI-type	The LALI-type is the set of parameters needed to specify a LALI mechanism, for either a computational or a natural biological process. As parameters are varied systematically in the computational model, these result in predictable pattern differences such as smaller or larger spots, smaller or larger spot separations, or spot to stripe transitions. (This is analogous to the combined effects of genotype and environment taken together, but excludes developmental noise.)
LALI-space	The set of all possible LALI-types.
Phenotype	A set of measured observables (e.g. morphometric quantities or “comparable units” [8]), selected from a larger set of all the possible observables that could be measured from a complex pattern or organism.
Phenotype Space	The set of all possible phenotypes, for the selected set of phenotypes (measured observables).
L→P Map	The LALI-type to phenotype map is the observed mapping, either computational or biological, from a set of LALI-types to a set of phenotypes. Due to random variation, one LALI-type can map to a set of phenotypes (see ‘phenotype cloud’), and many LALI-types can map to one phenotype (see ‘neutral region’).
Phenotype Cloud of a LALI-type	Due to stochastic factors in simulations (corresponding to developmental noise), a fixed set of LALI parameters can result in many different phenotypes. This set of phenotypes is the ‘phenotype cloud’ of that LALI-type. (This is roughly analogous to the concept of reaction norm in ecology and evolution.)
Neutral Region of a Phenotype	A phenotype can be produced by many LALI-types. The neutral region of a phenotype is the set of LALI-types that are likely to yield that phenotype. (This is analogous to the genomic neutral region of a phenotype.) We define the <i>r</i> % neutral region of a phenotype <i>P</i> as the set of all LALI-types <i>L</i> such that the <i>r</i> % phenotype cloud of the LALI-type includes the phenotype <i>P</i> .

<https://doi.org/10.1371/journal.pcbi.1006943.t001>

model of pattern formation, the *quantitative results* are model dependent (i.e. the numerical values depend on the specific chosen LALI model of pattern formation). To highlight this point, we include results for two different models based on reaction-diffusion equations, a linear one and a nonlinear one (see [Methods](#)). Comparison of the results for these two models allows for an illustration of the quantitative differences, but qualitative similarities, of the two models.

### Periodic color patterning in vertebrates: A likely developmental mechanism

Vertebrates show a wide variety of integumentary colors and patterns both within and among species. Variation in vertebrate coloration represents a model to understand the link between genetic basis, developmental patterns, and phenotype (e.g., [12–15]). Furthermore, variation in coloration is often under strong selection and linked to ecological or behavioral differences within and among species (e.g., [9, 16–19]). Although the genetic and developmental basis of vertebrate coloration have been identified for a few species (e.g., [12, 15, 20]), the mechanisms involved in color pattern formation in vertebrates are largely unknown (but see for example [21] and references therein; [22]), especially for vertebrates other than mammals or fish. While molecular approaches can uncover the genes involved in determining a certain color pattern (e.g., [20]), most of the time, especially for non-model species, the relationship between the candidate genes involved in color pattern formation, organization and variation and the observed phenotype are unidentified [15].

Strikingly, body color patterns with periodicity such as spots and stripes are found ubiquitously throughout vertebrates (studied most extensively among cats, fish, and some reptiles, see below) suggesting that mechanisms for periodic patterning may be very common, even universal, among vertebrates and thus their development conserved among organisms. The mechanism of ‘local activation long range inhibition’ (LALI; [23–25]) represents a general theoretical model predicting patterns that are spotted, striped or of an intermediate mixed form. The most important such mechanism is the Turing mechanism in reaction-diffusion system, where the local activation and lateral inhibition are due to reaction kinetics mediated by diffusion [26]. Murray was the first to propose an activator-inhibitor LALI mechanism for mammalian coat pattern formation [27–29], with the idea that a chemical pre-pattern established by a Turing-type mechanism dictates cell differentiation. Murray showed that many mammalian patterns observed in nature can be produced by such a mechanism. Turing-type mechanisms have since become a frequently studied and widely hypothesized mechanism for periodic patterning of integument in vertebrates (a wide array of mammals, including cats [16], several species of fish [22, 30–32] and reptiles, especially squamates such as snakes [9, 16, 33, 34] and recently a convincing ‘living’ (experimental) reaction diffusion model for skin color patterns in the ocellated lizard [35]).

Two key characteristics of patterns generated by LALI mechanisms are: 1) non-random regularity in the spacing of clustered elements (periodicity) and 2) potential for mixed transitions between spotted and striped patterns. Thus, the LALI model is suited to analyze periodic patterns and can provide a mathematical framework for analyzing pattern transitions between spotted and striped phenotypes. Many species of lizard and snake (squamate reptiles) demonstrate all of these pattern variations during ontogeny, within the same individual among the different parts (e.g., tail, trunk and head), and among individuals of the same or different species (YC pers. obs.). Among reptiles, the leopard gecko (*Eublepharis macularius*) shows particularly dramatic changes in pattern during maturation ([Fig 1](#)), transitioning from a hatchling pattern with alternating dark and light bands with a dark head to



**Fig 1. Ontogenetic pattern change in the leopard gecko (*Eublepharis macularius*).** Each photographed individual represents the typical color and pattern of a (A) hatchling (one month old), (B) juvenile (three months old), and (C) adult (>12 months old) gecko. Relative sizes are approximate, and the hatchling image has been enlarged to allow an easier comparison of pattern detail among individuals. Pictures by T. Gamble.

<https://doi.org/10.1371/journal.pcbi.1006943.g001>

an adult pattern consisting of a light colored body and head with scattered dark spots [36, 37]. Leopard geckos have been bred in captivity for decades and during that time numerous color and pattern mutations have been developed by private hobbyists [38, 39], providing a unique opportunity to understand how pattern variation can be created at the intraspecific level.

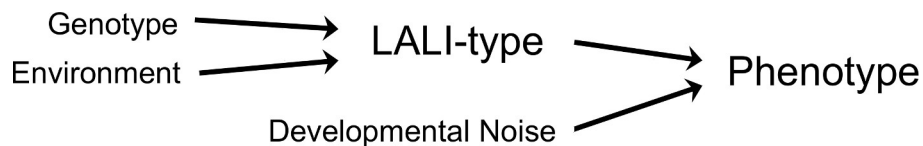
Since the leopard gecko demonstrates such a broad range of stage and body-plan-specific patterning, in this work, we focus on understanding the mechanisms generating the color pattern variation of a precise region on the leopard gecko head (the parietal, post-orbital region) during a specific stage of their development (at nine weeks). Among all the individuals analyzed in this study, this region of the head at nine weeks is invariably a simple spot pattern of discrete melanistic blotches on a pale background. At nine weeks of age the pattern spatial organization is determined and although the shape of the simple spots may continue to develop during the animal growth, the position of the spots and their relative organization is fixed. By analyzing images of the gecko head for the different individuals, we extracted key morphological features of the spotted pattern. These extracted features allowed us to compare the gecko's patterns with patterns obtained through LALI simulations: a simulation pattern and a gecko pattern were defined to be "matching" if they had the same values for these morphological features (see below). In this work, each LALI-type (see Table 1) corresponds to a

fixed combination of the contribution of genotype and environment to the developmental process and distinct LALI-types therefore represent different fixed combinations of genotypic and environmental values. We were able to find matches by varying LALI parameters (corresponding to changing genetic and environmental factors to another fixed state) for the eight experimentally observed gecko patterns within a low-dimensional LALI space (see definition in Table 1). By varying parameters within this region of LALI space, we were able to generate very likely, “normal” pattern variations. Furthermore, by expanding parameters just outside this region, we were able to generate “preternatural” pattern variations predicted by the developmental model just beyond the region of natural variation. These preternatural patterns are patterns that are not observed on the studied geckos, but are patterns that could potentially exist by varying the genotype and environment. These preternatural patterns in fact look like typical periodic patterns that are seen on animals, but they have morphological features with values that are slightly lower or higher than those we observed on the eight studied geckos.

**LALI-type to phenotype map  $L \rightarrow P$ .** Many mechanisms with the same core LALI logic (molecular, cell-based and/or mechanical) yield similar patterning despite different underlying biological processes [40]. While variations of reaction diffusion process are often used to explain Turing patterns, other candidate mechanisms include cell-based and mechanical processes [40]. In vivo, it has recently been established that Turing patterns on zebrafish skin are the result of a mechanism that satisfies the core LALI logic but that is qualitatively different from reaction diffusion [41]. With this perspective in mind, especially given that the molecular details of leopard gecko skin patterning remain unknown, our aim was to investigate mathematical features of LALI mechanisms in general rather than commit to a specific one. We therefore compared and contrasted results for two computational models—a model based on linear reaction dynamics (as in Turing’s classic paper [26]), and one based on FitzHugh-Nagumo reaction kinetics [42–44].

In biological systems, a LALI mechanism depends on physical quantities such as molecular diffusion rates, protein reaction rates, cell response rates, material resistance to bending and compression, etc. Computational LALI models aim to simulate the *net* effect of these physical quantities with a relatively small number of parameters. (For example, the Swift-Hohenberg equation can be seen as an approximation of a class of LALI models involving the net outcome of non-local effects [39].) By simulating the net effect of these physical quantities, pattern variation can be investigated without needing to fit a large number of unknown physical quantities. We stress that we do not claim that the equations in this paper model the specific biochemical processes occurring during gecko skin pigmentation, e.g. we do not assign specific identities to the chemicals in the reaction-diffusion equations. Rather, we use two different sets reaction-diffusion equations to generate prototypical LALI patterns. We note that a detailed model of the specifics of gecko skin pigmentation would need to address points such as the exact mechanism by which cells sense the external concentration and what effect this has on their genetic programs. These points are beyond the scope of our current investigation.

Given either a computational model of a LALI mechanism or a real world LALI mechanism (e.g., color patterning), the LALI-type (Table 1 for definition) to phenotype map  $L \rightarrow P$  is the map from parameters (see below) of the LALI model (‘L’) to a final phenotype (‘P’). It represents a developmental step that occurs after genotype and environment have determined the parameters relevant to the LALI mechanism (see Fig 2), for example after the environment and genotype determines which gene(s) should be activated, how much, and for how long in a certain body region. Varying the parameters of the LALI-type in simulations is analogous to varying the underlying genetic and environmental factors that specify the LALI mechanism (e.g., molecular, cell-based, mechanical) producing a certain phenotype in biological systems.



**Fig 2. Conceptual model of the LALI-type to phenotype map.** The LALI-type summarizes the genetic and environmental factors of a LALI pattern. The phenotype is a product of the LALI-type and stochastic effects (random variation called developmental noise).

<https://doi.org/10.1371/journal.pcbi.1006943.g002>

Furthermore, given either a computational model or an actual biological LALI mechanism, the spatiotemporal evolution of the pattern is influenced by developmental noise. Indeed, the diffusion-driven instability in both the linear model and the FitzHugh-Nagumo model relies on small, stochastic fluctuations of the micro-environment, just like any Turing-like instability in pattern formation mechanisms with a core LALI logic [40]. The diffusion-driven instability occurs through the amplification of these fluctuations and ultimately creates the Turing pattern of regions (e.g., spots or stripes) of high and low concentrations of some chemical (“peaks and troughs” [26]; or Turing “bifurcation” [41]). Such stochastic fluctuations enter the model through randomly perturbed initial conditions. The effect of stochastic variation in the computational LALI model is that the relationship between LALI-type and phenotype is not one-to-one, that is, even if genetic and environmental factors are fixed, a single LALI-type can generate different phenotypes and conversely different LALI-types may generate the same phenotype. Thus, this framework and a computational model of a LALI mechanism permit us to either vary genetic and environmental factors together as a unit or hold them fixed (by varying or fixing the parameters of the computational LALI model), and to investigate the outcome of the  $L \rightarrow P$  map. The outcome of the  $L \rightarrow P$  map for a fixed LALI-type would measure the variation due to noise within the developmental program, while the outcome for different LALI-types would measure the variation due to variation in genotype and/or environment without discerning between them. Specifically, the approach used in this work allows isolating the effect of the two different factors contributing to the total variation.

## Methods

### Pattern analysis and morphometrics of live geckos

**Ethics statement.** All experiments were carried out in accordance with University of Minnesota animal use protocols 0810A50001 and 1108A03545.

**Data collection.** Individual live leopard geckos were photographed within two weeks of hatching and subsequently photographed every two weeks thereafter to document pattern changes over time. Pattern change over time was however only considered in this work to select the developmental stage at which the spatial organization of the pattern was stable, and we could collect the data for this work. Each gecko was photographed on a smooth surface that featured a grid pattern with evenly spaced lines 12.7 mm apart. Photos were taken with a Sony DSC F828 8 megapixel camera mounted on a tripod approximately 45 cm above the gecko. One single photo per gecko was used in this study.

**Pattern selection.** For pattern analysis, we selected a disk-shaped region of the parietal, post-orbital head region of eight geckos at nine weeks (see [Introduction](#) regarding selection of chosen developmental time). A disk-shaped region was identified from images of the gecko head by an algorithm run in Matlab (Matlab R2015b, Mathworks, Inc.) that identified the largest disk that could be inscribed within the boundary of the head, for a disk centered at the centroid of the head. The size of the pattern disk varied for each gecko, but was invariably a

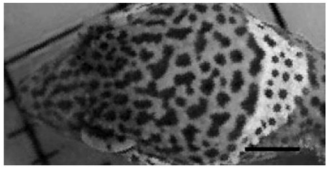

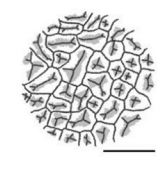
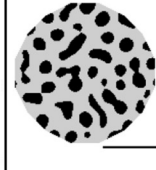
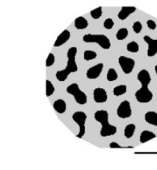
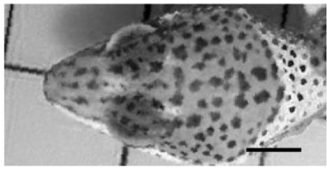


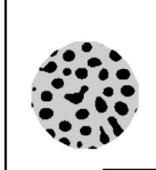

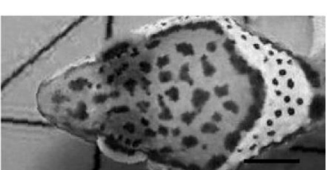







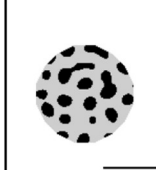



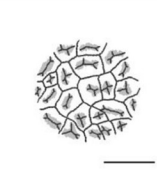





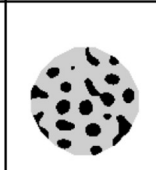

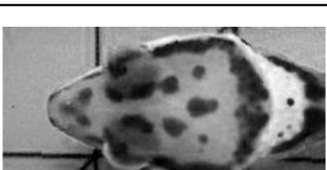

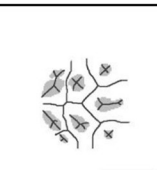
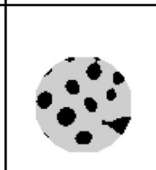

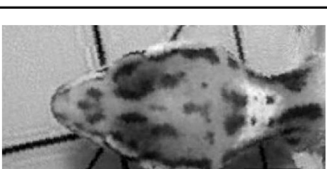


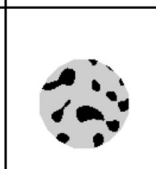

pattern of isolated melanistic spots on a lighter background. Images of the eight gecko heads and the corresponding selected disk-shaped regions are shown in the first and second columns of Fig 3. Focusing on this region restricted the image to one pattern type (discrete dark spots on a lighter background) in order to study a homologous region among individuals without including areas of the head where the pattern transitioned from one type of pattern to another. Head boundaries of the gecko were determined by hand, while identifying the centroid of the head and the largest inscribed disk was automated for the eight gecko images using Matlab.

### Image processing

Image processing of the live gecko images was required to correct for uneven lighting within and between photos, as well as different background levels of pigment from one gecko to another. Each disk-shaped image was contrast-enhanced (using Matlab's internal *adaptstretc* function) to correct for shadows and inconsistent lighting. A threshold was then applied to binarize the image into a set of black pixels on a white background. Since pigment levels varied for each gecko, a different threshold value of pigment was required to discriminate spots from non-spots. For each gecko, the threshold value was calculated from the average pixel intensity  $\mu$  and standard deviation  $\sigma$  of the pixel intensity. With experimentation, it was determined that a threshold of  $T = \mu - \sigma$  was high enough to detect spots yet also low enough to identify their separations (i.e. pixels were required to be a standard deviation darker than average in order to be identified as a spot pixel). Thus, while each image had a different threshold for discriminating spots from non-spots, a single, objectively set definition was used to define this threshold. It was observed that small changes in the threshold could result in the joining or separation of nearby spots. To describe the variation generated by small variations in the choice of threshold, the mean and standard deviation of pattern statistics were computed by varying the threshold by 25% of the standard deviation of the pixel intensity. Before computing final pattern statistics, pattern noise due to arbitrary threshold cut-offs was eliminated by 1) filling holes within spots and 2) deleting stray pixels outside of spots. Holes within spots were identified as pixels with intensity below the threshold that were nevertheless completely contained within a region of pixels identified as a spot. Stray pixels outside of spots for removal were identified by a total area that was too small to be identified as a spot (the cut-off was 10 photo pixels). For the calculation of the *peak length* (Table 2), we found that the image skeletonization generated by the native Matlab operation could be sensitive to the contour of spots. Since the peak length should only depend on the spacing of spots and not their contour, we first found the convex hull of the spots and then skeletonized the image (skeletonizations are shown in Fig 3, Column 3).

**Morphometrics: Selected phenotype specified by fractional area and eccentricity.** For the pattern selected from the chosen region of the gecko's head, we defined the *selected phenotype* of that pattern as the pair of numbers given by the *fractional area* and the *eccentricity* of the melanistic spots. The fractional area is a measure of the relative density of spots (pigmented regions) and the eccentricity of a spot is a measure of the pattern location on a spot to stripe continuum that is valid up until pigmented regions begin to overlap (see Table 2 for all definitions of technical terms used in this section). These two measures were chosen from an unlimited number of possible morphometric measurements to focus our analysis since these are measures that are readily interpreted in the context of periodic patterns (as measures of the relative spot or stripe size and position of the pattern along the spot to stripe transition), straightforward to vary with LALI parameters and are scale free, and thus not depending on the size of the individual gecko. For both live and simulated pattern images, statistics were measured using automated Matlab scripts (these scripts accept as input any disk-shaped region with a binary pattern of black and white pixels, and did not distinguish between simulated and live



	Gecko Head Pattern	Pattern Region	Pattern Skeletonization	Best Match (Linear)	Best Match (FitzHugh-Nagumo)
772					
681					
763					
731					
682					
732					
773					
735					

**Fig 3. Automated disk-shaped pattern selection of parietal, post-orbital head region of eight geckos at nine weeks.** For each Gecko ID (numbers on the left): Left: Images of the eight gecko heads at nine weeks; Second column: the disk-shaped parietal, post-orbital (DSPPO) region that was selected for pattern analysis, preserving their relative sizes; Third column: Final pigment pattern identified by image analysis with the skeletonization of the image overlaid. Fourth column: Best phenotype match of 100 patterns simulated by the corresponding LALI-type using the linear model. Right: Best phenotype match of 100 patterns simulated by the corresponding LALI-type using the FitzHugh-Nagumo model. Horizontal bars indicate 0.5 cm. Geckos are ordered by decreasing fractional spot area of the pattern (see Table 2 for definitions). Note that in some cases in the nonlinear model, the spots have a ‘ringed’ appearance. This is the result of morphogen profiles that have a maximum concentration around the border of the spots. We note that the lack of pigment in the interior is contingent upon finely tuned threshold values, which means that the robustness of these patterns to perturbations of the sensing mechanism of the cells is likely quite weak. Our search algorithm identifies sets of parameters that yield matches to specified pattern statistics (here, fractional area and eccentricity). While the algorithm may find that finely tuned thresholds give the best match, in future applications, additional prescriptions can be applied for a match such as requiring that the pattern matches are robust to small percent perturbations or that spots do not have interior holes.

<https://doi.org/10.1371/journal.pcbi.1006943.g003>

gecko patterns). For the live gecko images, we also measured the average spot size, a scale-dependent statistic which was used for fixing the spatial scale of simulated pattern images (see discussion below of the selection for the pixel spatial scale). We also calculated the average distance between spots (i.e., the *peak length* or *Fourier wavelength* of the pattern).

### Simulation-based generation of LALI patterns using two reaction diffusion models

We modeled the core LALI logic of an activator-inhibitor system using two model implementations. Comparing results for two implementations helps identify which aspects of the LALI-space to phenotype space map may be most implementation specific. We used a linear Turing model implemented on a discrete cellular automaton and the non-linear FitzHugh-Nagumo model. In both models,  $D$  describes the relative diffusion rate of the activator  $u$  and inhibitor  $v$ .

**Linear Turing model.** The equations for the linear Turing model are given by:

$$\frac{\partial u}{\partial t} = f_u u - f_v v + D \nabla^2 u$$

$$\frac{\partial v}{\partial t} = g_u u - g_v v + \nabla^2 v$$

The parameters  $D, f_u, f_v, g_u, g_v$  are fixed parameters that are initialized at the beginning of a simulation and do not change during the simulation. In an activator-inhibitor morphogen

**Table 2. Morphometric properties and how they were calculated.**

Pattern Statistic	Definition
Fractional Area FA	The fractional area is calculated as the total number of dark (melanistic) image pixels divided by the total number of pixels in a disk-shaped region.
Eccentricity EE	The eccentricity of a spot is a value between 0 (a perfect circle) and 1 (a perfect line) calculated using the <i>regionprops.m</i> Matlab subroutine.
Spot Size	The diameter of a spot was calculated using the <i>regionprops.m</i> Matlab subroutine and is the equivalent diameter of a circle with the same area as the spot.
Peak Length	The peak length, a measure of the average distance between pattern elements such as spots or stripes, was computed according to the method of [45] by finding the skeleton of the positive and negative of each image. Peak length was calculated by applying the following formula: $\text{Peak Length} = \frac{2 \times (\text{total image pixels})}{(\text{valley pixels}) + (\text{peak pixels})}$
Fourier Wavelength	Rectangular grayscale images with varying pixel intensities, scaled to have zero mean, were used rather than binarized images. The Fourier wavelength is the inverse of a radius that can be estimated from the Fourier spectrum (the magnitude of the coefficients of the Discrete Fourier Transform) that displays a typically ring-like structure. The radius of this ring was determined numerically by maximizing the radially averaged Fourier spectrum. As a measure of localization, we indicate the interval in which the radially averaged Fourier spectrum is within 90% of its peak value. (See Supplementary S1 Fig)

<https://doi.org/10.1371/journal.pcbi.1006943.t002>

context, the parameters  $f_u, f_v, g_u, g_v$  are understood, respectively, as the self-upregulation rate of the activator, the down-regulation rate of activator by inhibitor, the upregulation of inhibitor by activator and the self-down-regulation of inhibitor, respectively, while  $D$  is the ratio of diffusion coefficients of the activator and the inhibitor.

Stochasticity is incorporated by initial conditions of random morphogen concentrations (initial concentrations of the activator  $u$  and inhibitor  $v$ ), with random values uniformly distributed between 0 and 1. Simulations were run on a patterning domain consisting of a  $200 \times 200$  spatial grid with periodic boundary conditions for a fixed number of time steps (200K). Note that the final morphogen concentrations generated by our simulations are not steady states, since simulations are stopped at a fixed number of simulation time steps. In simulations, pigmented regions transitioned from loosely defined and labyrinthine regions, to well-separated pigmented regions of high eccentricity, to more and more disk-shaped regions (see S2 Fig). To approximately match the eccentricity of the gecko spots, 200K time steps was an intermediate time point when the pigmented regions of the pattern were well-defined and discrete but not yet too disk-like. For all simulations for linear reaction diffusion in this manuscript, we fix  $f_v, g_u, g_v$  and used the production rate of the activator  $f_u$  as a parameter for pattern matching (see “Step 2” of the Results). As a second parameter, we also varied the threshold value of morphogen that would map to whether a region was pigmented (see below).

**FitzHugh-Nagumo model.** The equations for the FitzHugh-Nagumo model are given by the following nonlinear reaction-diffusion equations:

$$\frac{\partial u}{\partial t} = -(u - R)(u^2 - 1) - \rho(v - u) + D\nabla^2 u$$

$$\frac{\partial v}{\partial t} = -(v - u) + \nabla^2 v$$

Here  $D$ ,  $R$  and  $\rho$  are parameters, where  $D$  is the ratio of diffusion coefficients of the activator and the inhibitor,  $\rho$  is related to the relative rates of production of the activator and the inhibitor and  $R$  is a reference activator concentration. There are three steady states given by  $u = v = +1$ ,  $u = v = -1$ , and  $u = v = R$ . We note that in order to expand the reaction kinetics close to the steady state  $u = v = R$ , we can introduce new variables  $U = u - R$  and  $V = v - R$  and obtain the equivalent system:

$$\frac{\partial U}{\partial t} = (-R^2 + 1 + \rho)U - \rho V - 2RU^2 - U^3 + D\nabla^2 U$$

$$\frac{\partial V}{\partial t} = U - V + \nabla^2 V$$

It is known that for certain ranges of parameters, the equations can produce stable spots or stable stripes in two dimensions. Whether stable stripes or spots exist depends on the quadratic and cubic terms [46, 47]. For instance, if the quadratic term is zero (i.e.  $R = 0$ ), it is known that spots are unstable and stripes are stable [47].

We fixed  $R = 0.047$  and  $D = 0.0194$  and used  $\rho$  as a parameter for pattern matching. As a second parameter, we also varied the threshold value of morphogen that would map to whether a region was pigmented (see below). Stochasticity is incorporated by initial conditions of random morphogen concentrations. (The steady state  $u = v = -1$  was perturbed by uniformly distributed, spatially uncorrelated perturbations of amplitude 0.25 at each grid point of the  $200 \times 200$  spatial grid.) The equations were solved with the method of lines on a square of side length  $L = 20$  with no-flux boundary conditions, using Matlab’s differential equation

solver *ode45* (grid size of the discretization was  $200 \times 200$ ) on a fixed time interval  $[0,20]$ . The final morphogen concentrations generated by our FitzHugh-Nagumo simulations are not necessarily steady states, since simulations are stopped after a fixed time interval.

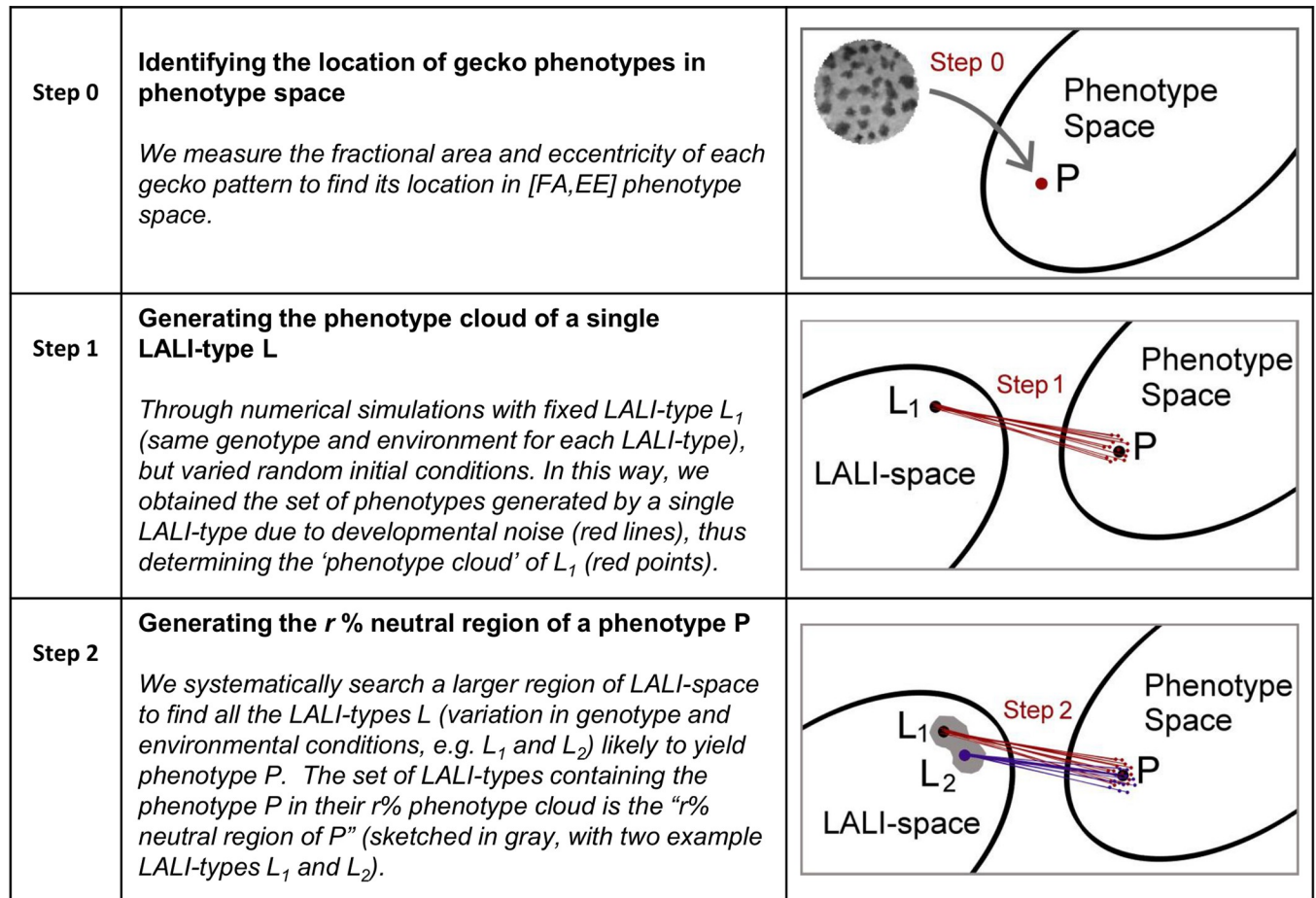
**Total set of varied model parameters.** For a complete list of model parameters, besides the set of parameters needed to initialize and run the simulations, we also needed to specify the threshold value of morphogen that would map to whether a region was pigmented (see below). Including this threshold parameter, the LALI-type for our linear model is completely specified by the six parameters  $[D, f_u, f_v, g_u, g_v, T]$  and the LALI-type for the FitzHugh-Nagumo model is completely specified by the four parameters  $[D, R, \rho, T]$ . In this project, we reduced the dimension of our search space by only varying  $f_u$  and  $T$  in the linear model and  $\rho$  and  $T$  in the FitzHugh-Nagumo model, as this was sufficient to find pattern matches for all eight gecko patterns.

**Modeling developmental noise.** As described above, for both computational models, stochasticity is incorporated by initial conditions of random morphogen concentrations. Other, more detailed approaches to modeling the sources contributing to developmental noise exist. For instance, intrinsic cellular noise (the stochasticity of gene expression within single cells), can be modeled via simulations using the Gillespie stochastic simulation algorithm [57,58, 59]. Extrinsic noise (the stochasticity of gene expression varying across different cells) can be modeled for example by stochastic differential equations [60]. These and other sources of developmental noise are varied and complex. Noise intrinsic to cells such as noisy transcription is an important contributor to developmental noise, but also other factors at the molecular level, at the developmental systems level and the organismal level (noisiness in gene interactions within and between regulatory networks, or noise in cell to cell signaling) are thought to contribute to developmental noise [11]. Many of these contributing factors and their significance are poorly understood. It is because of this complexity that we do not seek to model each of these contributions by itself, but rather see the random initial conditions as a high-level approach to modeling noise.

Final LALI spot patterns, simulation image analysis and Pattern Statistics: For both the linear and non-linear reaction diffusion models, simulations within an appropriate range of parameters resulted in a spatial pattern of low and high morphogen concentrations. Note that the final morphogen concentrations generated by our simulations are not steady state morphogen concentrations, but instead capture the pattern at an intermediate time point. For more details on the time evolution of the simulated patterns, and a description of the effect of varying the simulation end point and other parameters on the spot eccentricity, see S2, S3, S4 and S5 Figs.

Morphogen concentrations after a fixed number of simulation steps (200K steps for the linear model, time interval  $[0,20]$  for the FitzHugh-Nagumo model) were binarized into distinct regions of spots and non-spots using a threshold parameter  $T$  to produce a black and white pattern. In principle, the applied threshold parameter  $T$  in the computational models would correspond to the threshold concentration of morphogen for which biological cells produce pigment. The fractional area and eccentricity of the spots were calculated, for the entire simulated domain. Since fractional area and eccentricity are spatial-scale invariant, the generated  $L \rightarrow P$  map that maps from model parameters to  $[FA, EE]$ -phenotype space is also scale-invariant, and we consider that the absolute spatial scale of the pattern is a free parameter.

Cutting disk-shaped regions of simulated patterns: For generating the simulated phenotype matches in Fig 3 and determining the intrinsic variability of each of the eight phenotypes in Fig 10, disks were cut from simulated domains to match the relative domain-to-pattern spatial scales of each of the eight phenotypes. First, since the spatial scale of a pixel in simulated patterns is a free parameter, the spatial size of a pixel was set so that the average size of spots in the



**Fig 4. Overview of methods (Steps 0–2).** The L→P map is modeled by one of two computational reaction diffusion models. Due to developmental noise, one LALI-type probabilistically maps to many phenotypes (the ‘phenotype cloud’) and many LALI-types map to one phenotype (the ‘neutral region’ of the phenotype).

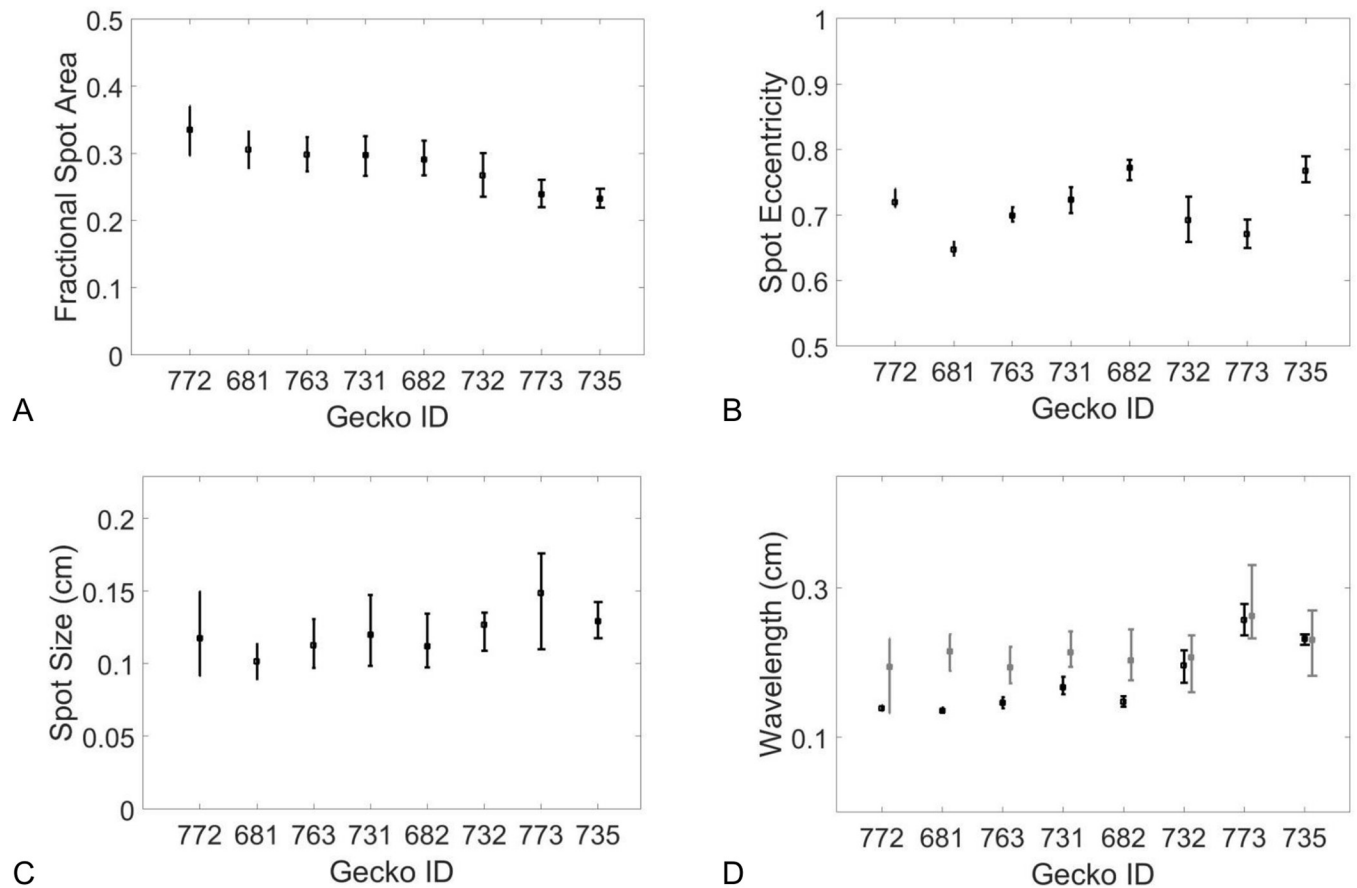
<https://doi.org/10.1371/journal.pcbi.1006943.g004>

simulated pattern would match those of the gecko phenotype. Once the spatial scale was established in this way, a disk was cut from the simulated pattern with the same radius as that of the gecko image. This was an important step to ensure that simulated phenotype matches contained, for example, the same number of spots when other statistics such as the fractional area and eccentricity matched. For these disk-shaped regions cut from simulated larger domains, the fractional area and eccentricity of the spots was measured using the same automated scripts as for the live gecko images.

While the LALI-type determines pattern characteristics such as the average fractional area and eccentricity, the domain size of the pattern is relevant because this determines the amount of the pattern that is captured (actual number of spots). A disk-shaped post-orbital head region with domain size that is relatively small compared to the pattern wavelength will have relatively few spots and will be a relatively small sample of the pattern.

### Generating the LALI-type to phenotype map by identifying the neutral region of each phenotype and the phenotype cloud of points in LALI-space

To investigate how a produced pattern (the phenotype) depends on the input parameters used for the simulation (the LALI-type), we consider the concept of the LALI-type to phenotype



**Fig 5. Spot statistics for each Gecko ID.** For each binarized image of spot patterning, A) fractional spot area, B) mean spot eccentricity, C) mean spot size and D) wavelength calculated by peak length (black) and Fourier (gray) methods were calculated. Geckos are ordered by decreasing fractional area. Error bars show the minimum and maximum measures of these measures as the threshold for binarization was varied by  $0.1\sigma_i$  where  $\sigma_i$  is the standard deviation of the image pixel intensity.

<https://doi.org/10.1371/journal.pcbi.1006943.g005>

map, or  $L \rightarrow P$  map (Table 1). More formally, a computational model for a LALI mechanism capable of describing a range of patterns of interest can be defined with a set of model parameters  $\lambda_1, \lambda_2, \dots, \lambda_n$  and a set of rules for evolving the system to generate a pattern. The resulting pattern can be described with a set of morphometric measurements  $\rho_1, \rho_2, \dots, \rho_m$ . We consider that the vector  $(\lambda_1, \lambda_2, \dots, \lambda_n)$  is a point in LALI-space (referred as the “LALI-type”) and that the vector  $(\rho_1, \rho_2, \dots, \rho_m)$  is a point in phenotype-space (the phenotype) so that the computational model represents a mapping from LALI-space  $L$  to phenotype-space  $P$ .

Due to the element of random variation in the pattern generation process, a single LALI-type can generate different phenotypes, the ‘phenotype cloud’ of that LALI-type. Likewise, a particular phenotype can be produced by different LALI-types—the region of LALI-space containing this set of LALI-types is the ‘neutral’ region of that phenotype. We describe the LALI-type to phenotype map with the following steps (schematically summarized in Fig 4):

**Step 0:** We identify the phenotypes of the eight live gecko patterns, for a small set of selected morphometric measurements, as described above. These phenotypes are points in phenotype space.

**Step 1: Generating phenotype clouds and defining the set of likely phenotypes** For a given LALI-type, its phenotype cloud is the corresponding distribution of measurements in

phenotype space generated from the patterns simulated for that LALI-type. The size of the phenotype cloud describes the role of random variation (developmental noise) for a fixed LALI-type. We define the ‘center’ of a phenotype cloud as  $(\hat{\rho}_1, \hat{\rho}_2, \dots, \hat{\rho}_m)$  where  $\hat{\rho}_i$  is the average value of the  $i^{\text{th}}$  morphometric measure. The center of the cloud and the probabilistic distribution of phenotypes within the cloud are used to define the set of ‘likely’ phenotypes: a phenotype is *likely* if the distance from the phenotype and the center of the phenotype cloud is closer than a specified fraction of the phenotypes in the phenotype cloud. With a pre-specified cut-off, this eliminates phenotype outliers that occur with smaller probability. We define the “ $r$  % phenotype cloud” as the subset of the total phenotype cloud that includes the  $r$ % of the phenotypes which are closest to the center. So, points that lie within the 50% phenotype cloud are those phenotypes whose distance from the center is less than the median distance.

**Step 2: Generating neutral regions of a phenotype** We identify neutral regions of each phenotype in LALI-space. This is describing the way the  $L \rightarrow P$  map maps *from* regions in LALI-space.

Given a specific pattern phenotype, the *neutral region* of that phenotype is the set of parameters in LALI-space that are “likely” to yield patterns with that given phenotype (using the metric provided from step 1). To systematically find the neutral region of each phenotype, we first identified a region of LALI-space that is capable of producing all eight phenotypes. Conveniently, we achieved this within a relatively low two-dimensional projection for both LALI models. The  $r$ % neutral region of a point  $P$  in phenotype space is then defined as the set of LALI-types  $L$  within this region for which  $P$  lies within the  $r$ % phenotype cloud of  $L$ . The larger the parameter  $r$ , the larger the size of the neutral region.

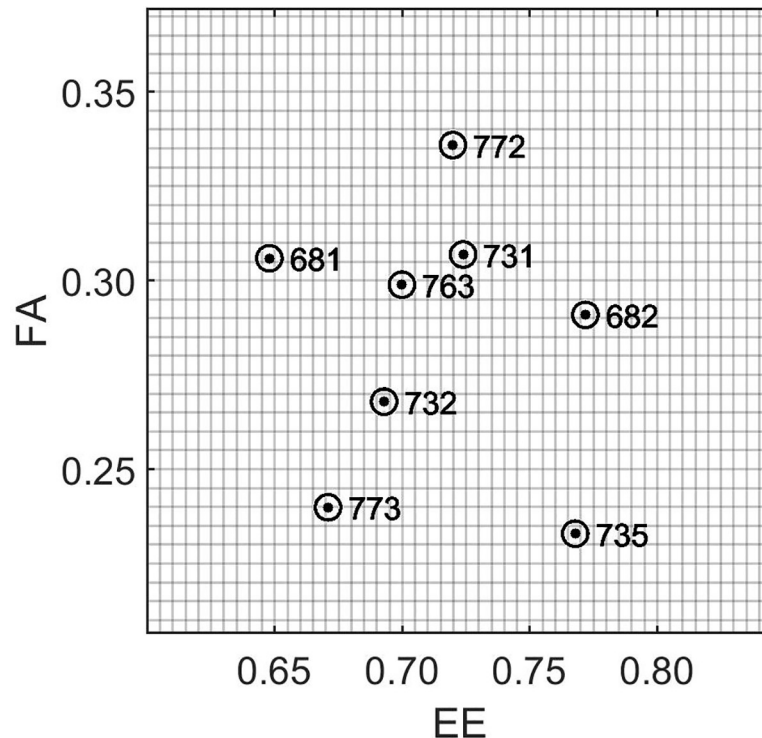
## Results

### Statistical image analysis of the eight live gecko patterns

Fig 5 shows how the phenotype measures varied for each gecko: the fractional pigmented area  $FA$  of the spots in each pattern (Panel A), the average eccentricity  $EE$  of the spots in each pattern (Panel B), the average spot size  $S$  in centimeters for each pattern (Panel C) and the pattern wavelengths (Panel D). The error bars show the dependence of the statistic on the pigment threshold that was chosen to decide if a gray pixel was either white or black. For our analyses (except for the Fourier wavelength), the single threshold of  $T = (\mu - \sigma)$  was applied, generating one binary image per gecko photo, so that the value indicated by each filled dot in Fig 5 is the actual value of morphometric parameters in each of the eight images that were used. The spot size was especially sensitive to the threshold that was chosen to binarize the image (relatively large error bars), whereas the measures of the wavelengths of the patterns (average distances between pigmented regions) were robust to this parameter. That is, the size of spots would be larger or smaller depending on whether pixels of intermediate intensity located at the edge of a blotch were classified as pigmented or not. The peak length and Fourier method gave similar measures of the wavelength; however, we speculate that systematic differences might be due to the way the methods average over wavelength variation across the image. For example, based on the way they are calculated, the Fourier wavelength would be biased towards the larger wavelengths whereas the peak length method would be biased towards the shorter wavelengths. The skeletonizations used for calculation of the peak length method are shown in Fig 3, Column 3.

#### Step 0: Identifying the location of the eight gecko patterns in phenotype space

For the spot patterns selected from eight live geckos, a set of automated scripts calculated the fractional area ( $FA$ ) and the eccentricity ( $EE$ ) of the pigmented spots. The selected *phenotypes* of the eight live gecko patterns, defined as the [fractional area, eccentricity]-pair [ $FA$ ,  $EE$ ]



**Fig 6. Location of the eight gecko patterns in FA-EE phenotype space.** The distribution of the eight patterns in [FA, EE] phenotype space where FA is the fractional area of spots and EE is the average eccentricity of the spots.

<https://doi.org/10.1371/journal.pcbi.1006943.g006>

located the eight gecko patterns in a two-dimensional [FA, EE]-phenotype-space ('Step 0', see Fig 4). The locations of the eight gecko patterns in [FA, EE]-phenotype-space is shown in Fig 6. For the eight live gecko patterns, the fractional area varied from 0.23 to 0.34, while the eccentricity varied from 0.65 to 0.77.

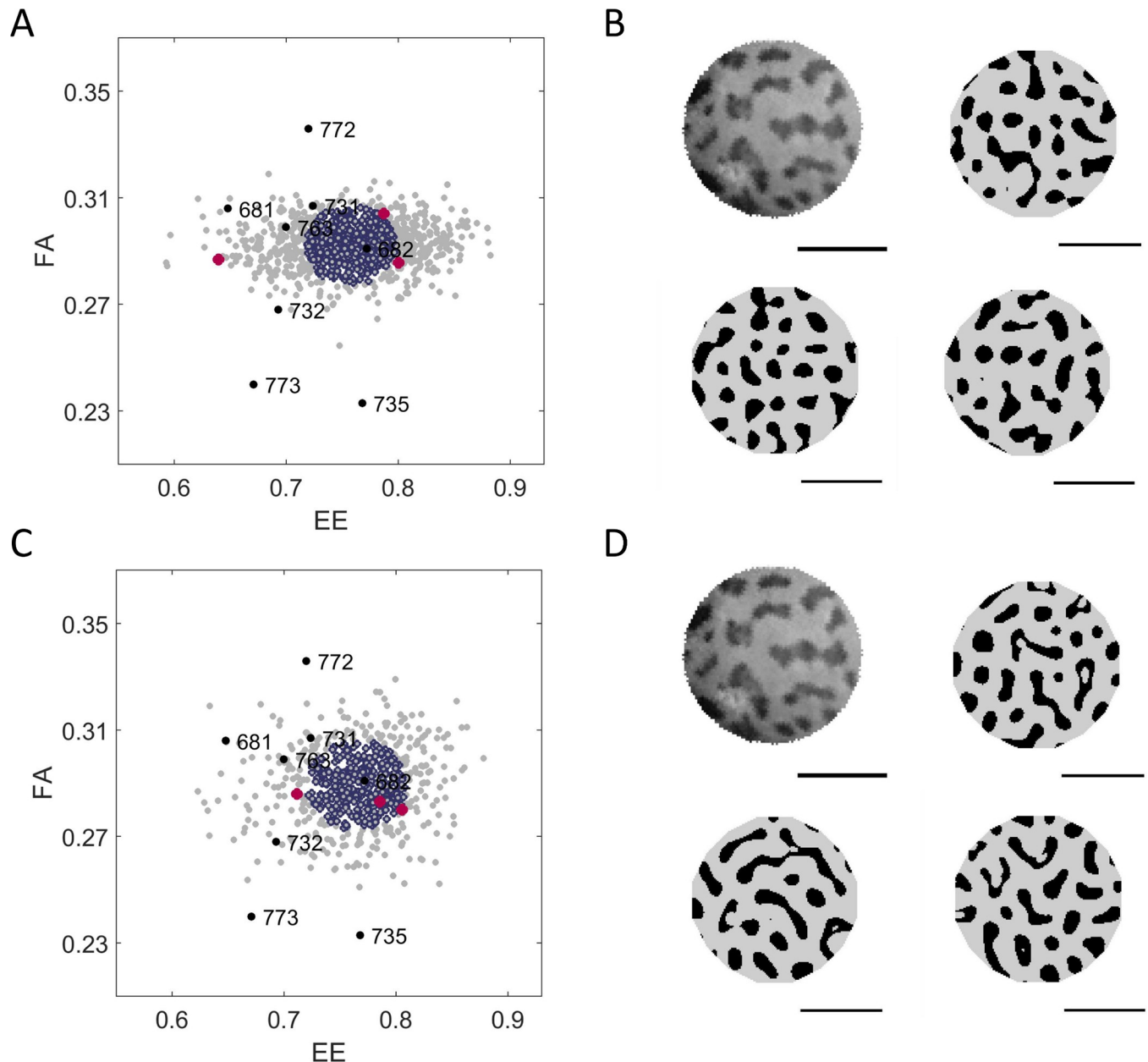
**Describing the LALI-type to phenotype map (via the identification of the neutral regions and phenotype clouds of the  $L \rightarrow P$  map).**

**Step 1: Generating the phenotype cloud of a LALI-type**

To illustrate the variation that would occur for a point in LALI-space due to random variation alone, we generate the phenotype cloud of a fixed point in LALI-space (single LALI-type) by simulating 1000 patterns at that location in LALI-space. As an example, Fig 7 shows a phenotype cloud of the linear (Turing) LALI map for the LALI-type  $[f_u, \hat{T}] = [0.811, 1.20]$  (Panel A) and a phenotype cloud of the non-linear (FitzHugh-Nagumo) LALI map for the LALI-type  $[\rho, T] = [2.63, 1.56]$  of (Panel B). The 1000 patterns generated create a cloud in [FA, EE]-phenotype space due to stochasticity since the LALI-type, and thus all LALI parameters, were held fixed. These points in LALI-type mapped to a phenotype cloud approximately centered on the phenotype of the gecko pattern #682 (the black point labeled 682 on Panels A and B).

In Fig 7, in Panels A and B, the phenotypes of points that are most likely (within the radius of a disk containing 50% of the point distribution) are outlined in purple. The phenotype for the gecko pattern #682 is well within this radius. Thus, the two chosen LALI-types are points that would potentially generate gecko pattern #682 for each model. In Fig 7, Panels C and D, gecko pattern #682 is shown with three patterns that were randomly selected from within the phenotype clouds of each LALI-type. Within the context of our modeling framework, the





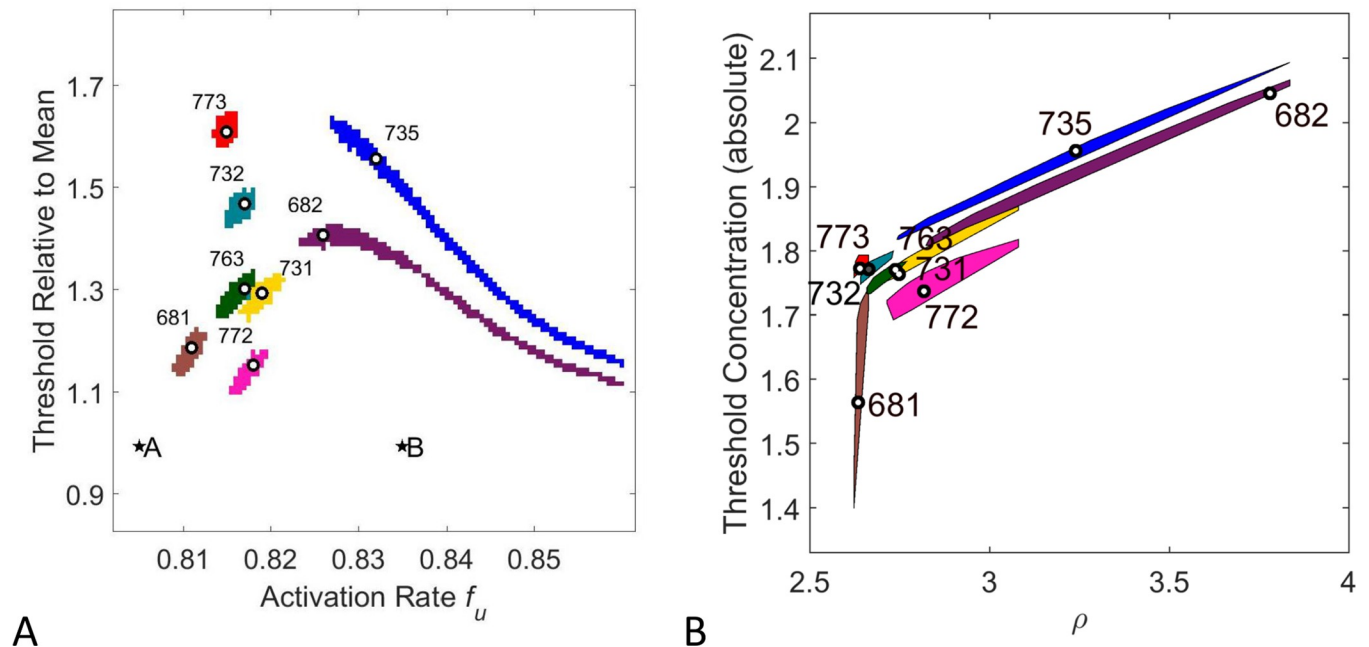
**Fig 7. Random phenotypic variation.** The phenotype cloud for 1000 simulations showing the random variation of a single LALI-type, for either the A) linear or B) FitzHugh-Nagumo models. The representative LALI-type was chosen from the 50% neutral region of gecko pattern #682. (The location of this LALI-type is shown as a labeled white dot in Fig 8). The phenotypes of the 1000 simulations are indicated as gray disks in FA-EE phenotype space, while the 500 within the 50% radius of the phenotype cloud are outlined in purple. Three random phenotypes from the cloud are shown in red (see below). C, D) The pattern isolated from the image of Gecko #682 and the patterns of three simulated “clones” (patterns generated with the same LALI-type that is likely to yield pattern #682, but allowing random variation). The result is not necessarily ‘close’ to the pattern #682 (their locations in FA-EE space are indicated in red in the panels ‘A’ and ‘B’). Horizontal bars indicate 0.5 cm.

<https://doi.org/10.1371/journal.pcbi.1006943.g007>

variations among these patterns correspond to the random variation of genetic and environmental clones.

**Step 2: Identification of the neutral region for each phenotype**

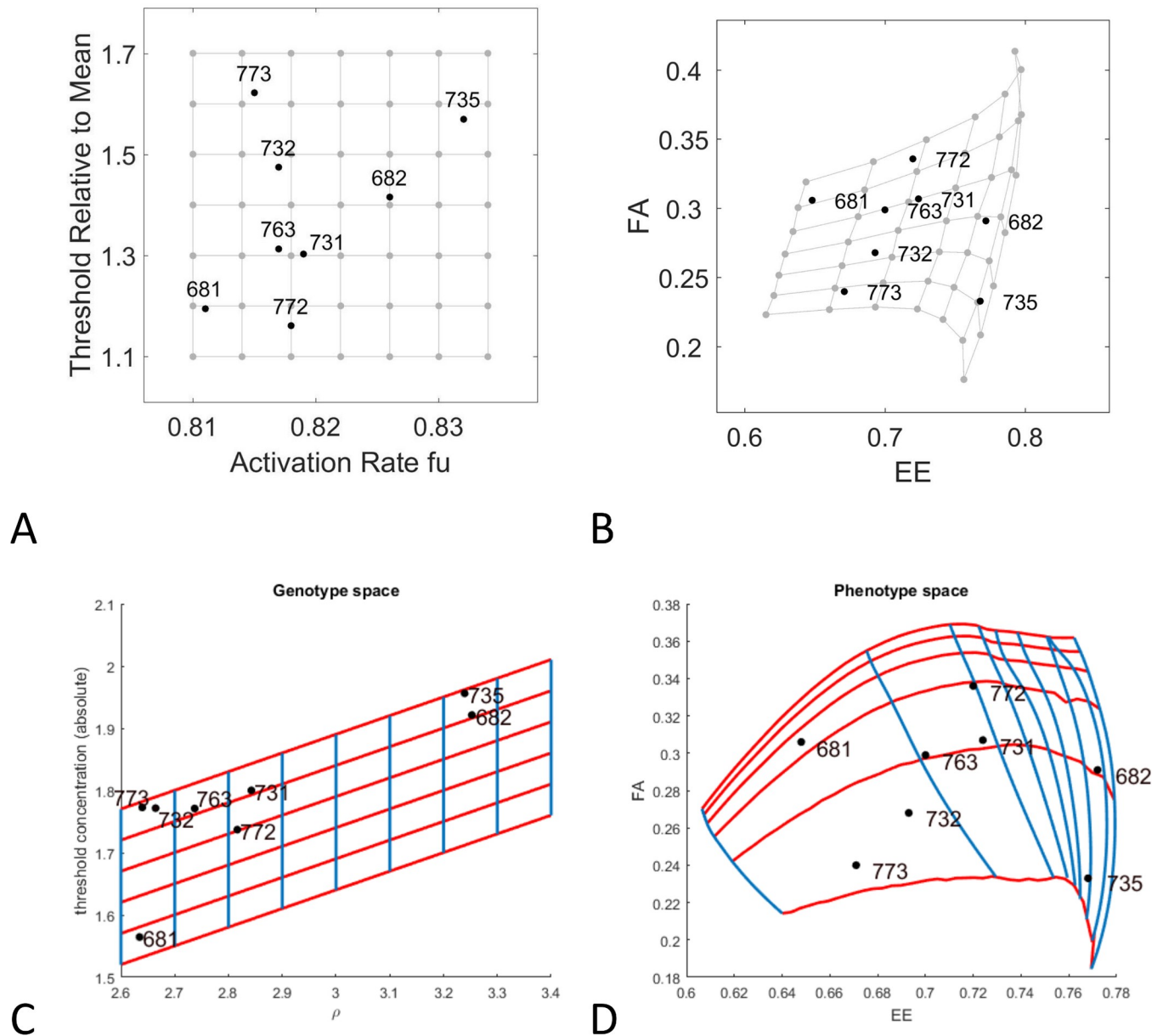
For each of the eight phenotypes identified, we recovered a region in LALI-space that was able to produce all eight phenotypes. This corresponds to a range of genetic and environmental



**Fig 8. 50% Neutral regions of each of the eight gecko patterns in LALI-space.** For each of the eight gecko patterns, we identified the neutral region A) in  $[\hat{T}, f_u]$ -LALI-space for the linear Turing implementation or B) in  $[T, \rho]$  LALI-space for the non-linear FitzHugh-Nagumo model. The white circle in each neutral region shows the LALI-type chosen to generate representative phenotype clouds in Fig 7 and Fig 10. The labeled stars A and B are the points in LALI-space that are used to generate the “*preternatural*” patterns in Fig 12. (Both models used the 50% phenotype cloud to generate the 50% neutral region, see the description under “Step 2” in the Methods).

<https://doi.org/10.1371/journal.pcbi.1006943.g008>

variation that can produce all eight phenotypes. For both models, we found that it was sufficient to only vary two LALI parameters. In principle, we would expect that the addition of other morphometrics, measuring more subtle patterns features, could require the variation of a greater number of LALI parameters for fitting more subtle pattern details. For the linear model, we varied the threshold morphogen value  $T$  and the activation rate  $f_u$ . For the Fitz-Hugh-Nagumo model, we varied the threshold morphogen value  $T$  and the model parameter  $\rho$ . For example, for the linear model, the identified region in LALI-space able to produce all eight phenotypes was a region in which the activation rate varied from 0.80 to 0.84 and the threshold morphogen value relative to the mean morphogen value ( $\hat{T} = T/\mu$ ) varied from 1.1 to 1.7. The 50% neutral region of each phenotype was identified by searching systematically within this region of LALI-space. Here a LALI-type lies in the 50% neutral region of a phenotype if the phenotype is closer to the center of the phenotype cloud than 50% of the points in this cloud. This means that the phenotype is closer to the ‘typical’ pattern than at least half of the possible patterns. Thus the 50% neutral region of a phenotype can be thought of as those LALI-types that yield a pattern similar to that of the phenotype with high probability. The 50% neutral regions of eight live gecko phenotypes are shown in Fig 8. We found that the 50% neutral regions were all non-overlapping with each other. In principle, the neutral regions might have overlapped if two geckos in the cohort had especially similar patterning. The 50% neutral regions of the phenotypes corresponding to the geckos labeled #763 and #731 nearly overlapped, but shared no grid points in common. The regions of LALI-space shown in Fig 8 (Panel A and B) were extended to show more of the neutral regions of #735 and #682 but these are still cut off in the panels because the neutral regions of #735 and #682 are so elongated. The relative elongation of the neutral regions of #735 and #682 indicate that matching the



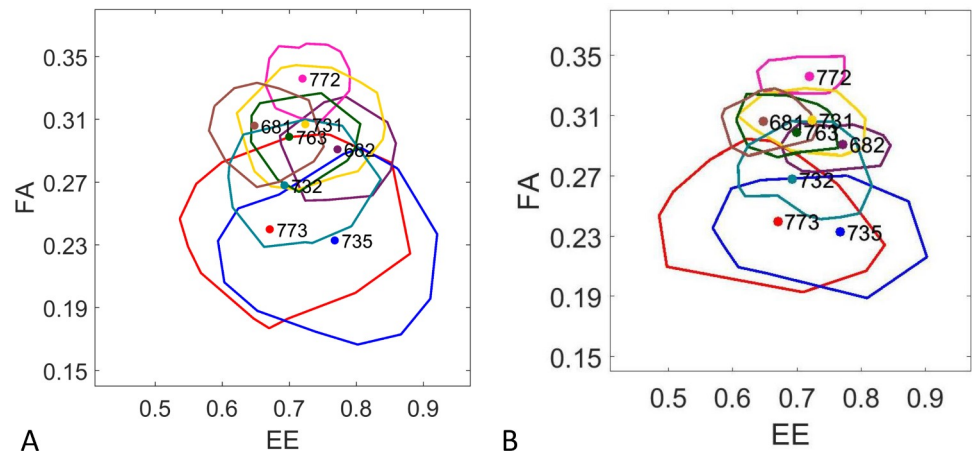
**Fig 9. Bias of the LALI-space to phenotype space mapping.** A regular grid containing points from the neutral regions of the eight gecko patterns is chosen and the mapping of that grid to phenotype space is shown. A rectangular grid A) in  $[T, f_u]$ -LALI-space for the linear Turing implementation or C) in  $T, \rho$  LALI-space for the non-linear FitzHugh-Nagumo model and the mapping of that grid in FA-EE-space for the B) linear Turing map and D) the non-linear FitzHugh-Nagumo model. The gray region indicates 25% of the area in LALI-space, which maps to a smaller fractional area in phenotype space. This corresponds to a higher likelihood of points (a higher density) in that region of phenotype space.

<https://doi.org/10.1371/journal.pcbi.1006943.g009>

phenotype is tolerant to varying the parameters  $f_u$  or  $\rho$  over a wide range, whereas in other regions of LALI-space the pattern is more sensitive to small changes in these parameters.

**The LALI-type to phenotype map enhances understanding of intra-group variation.**

For both implementations of the LALI-type to phenotype map, the linear Turing model and the FitzHugh-Nagumo model, we show the mapping of a regular grid in LALI-space to the corresponding region in phenotype space. Here a point in LALI-space is mapped to the coordinates of the center of its phenotype cloud in FA-EE-space. The regular grid lines in LALI-



**Fig 10.** The Intra-Group Variation of the Eight Leopard Gecko Pattern is Larger than Random Variation Each closed curve shows the outer contour of the 95% phenotype cloud for eight LALI-types that were selected from within the neutral region of each leopard gecko pattern for the A) linear Turing and B) FitzHugh-Nagumo models. These LALI-types are indicated in LALI-space as labeled white dots in Fig 8. Although the phenotype clouds overlap, even the largest phenotype clouds do not contain all of the phenotype variation of the group, indicating that the random variation is not large enough on its own to account for all of the variation.

<https://doi.org/10.1371/journal.pcbi.1006943.g010>

space are lines along which one parameter in LALI-space is held constant. For example, the horizontal grid lines in Panel A of Fig 9 (red lines) are lines along which  $\hat{T}$  is held constant and these map to non-linear curves in FA-EE-space (red curves in Panel B). Along each of these red curves in Panel B, the value of  $\hat{T}$  is held constant and each curve shows the effect of varying the parameter  $f_u$ . The extent to which these curves deviate from a pattern of parallel evenly spaced lines shows the extent to which there is  $\hat{T} \times f_u$  “interaction” (in the sense of statistical interaction, where interaction is the extent to which the effect of the parameters is not additive [48]). Regions of the map where these curves deviate from parallel straight lines are regions where there is more interaction. As an example of one way to interpret these isoclines, if one LALI parameter was genetically controlled and one parameter was environmentally controlled, this is the shape that the G×E interaction would take (see [49]). Both computational models predict that the T-isoclines (red-lines) particularly deviate from straight, parallel lines when the eccentricity is high, and the fractional area is low (lower right corner of the grid). Phenotypes in this area of phenotype space (#682 and #735) would be most differentially affected by small changes in the LALI-parameters (corresponding to genotype and environmental variation).

Describing the bias introduced by the LALI-type to phenotype mapping

There is a mapping bias for higher eccentricities and lower fractional areas (Fig 9). To aid in interpreting the bias, we can consider the hypothetical that the parameters randomly vary in the indicated region of LALI-space so that each grid area has an equal probability of being represented by a gecko offspring. However, this does not correspond to equal probabilities of encountering the regions in phenotype space. All the points in the region colored in gray in LALI-space (25% of the total area) map to a relatively small region in phenotype space. This translates to a relatively high probability of points clustering in that region in phenotype space (25% of the points would land in that gray region). In other words, even if the values in LALI-space were randomly varied around a central position, they would map to a phenotype that is skewed towards higher eccentricity and lower fractional areas. Without knowing of this underlying bias introduced by the LALI map, this clustering would be interpreted as a “designed” or purposeful clustering in phenotype space rather than a random one.

Another way of perceiving the bias is that gecko patterns that seem relatively well-separated in phenotype space (e.g., #735 and #682 in Panels C and D) could be found to have a relatively small separation in LALI-space. The relatively small differences in LALI-space result in large differences in phenotype space. Even if one phenotype had a selective advantage over another, it might be difficult to control which phenotype would arise. Also, differences in patterns may be more due to chance than would be expected just by looking at their distances in phenotype space (see also [Discussion](#)).

### Application of the L→P map: Interpreting the intra-group variation in the context of the random variation

Simulations for the same LALI-type yield a range of patterns due to random variation. We investigate and compare the intrinsic variability of each the eight gecko patterns by generating the distribution of patterns for each phenotype that would be expected due to random variation. For each phenotype, we generate a distribution of patterns using a LALI-type selected from their neutral region, and crucially we also restrict the domain size of the generated patterns to match that of the gecko pattern under study (see [Methods](#)). While the LALI-type determines pattern characteristics such as the average fractional area and eccentricity, the domain size of the pattern is relevant because this determines the amount of the pattern that is captured (actual number of spots). A disk-shaped post-orbital head region with domain size that is relatively small compared to the pattern wavelength will have relatively few spots and will be a relatively small sample of the pattern.

[Fig 10](#) shows the outlines of these phenotype clouds for all eight LALI-types, with clouds approximately centered at each phenotype. Here the outline of the 95% phenotype cloud is shown for both the linear and FitzHugh-Nagumo models, see the description under “Step 2” in [Methods](#). Due to both random variation and the restricted sample size of the number of spots on the individual gecko heads, there is extensive overlap of phenotype clouds and several LALI-types are capable of producing more than one of the eight gecko phenotypes. The potential of one LALI-type to produce more than one of the observed live geckos phenotypes is shown by the inclusion of more than one phenotype in the outline of a phenotype cloud. For example, the LALI-type producing the cloud centered at gecko pattern #735 is also capable of producing a phenotype like that of gecko pattern #773 or even gecko pattern #732 (with a lower probability) ([Fig 10](#)). Although there is extensive overlap among the phenotype clouds, no single phenotype cloud includes all of the eight gecko patterns. Thus, the variation between the gecko patterns is larger than that of random variation, even when the domain size of the pattern is considered. By defining the radius containing a specified percentage of each phenotype cloud, one can determine the relative likelihood that a phenotype could be generated by a single LALI-type due to random variation. We observe that LALI-types mapping to phenotype clouds in different regions of phenotype space have phenotype clouds with different sizes, corresponding to different amount of random variation intrinsic to that set of LALI parameters.

A domain size that is relatively small compared to the pattern wavelength will have relatively few spots; this is a relatively small sample of the pattern and the intrinsic variability of that phenotype will larger. For example, gecko patterns #735 and #773 are both especially small and have an especially large distance between spots, so that the patterns contain very few spots. Due to the effects of relatively small domain size, these phenotype specimens have the largest intrinsic phenotype variability.

The inclusive relationships of the phenotype clouds in [Fig 10](#) also allow for a description of the estimated likelihood that two gecko phenotypes correspond to the same LALI-type. The corresponding relatedness of pairs of phenotypes is given in [Fig 11](#). Here we determined for

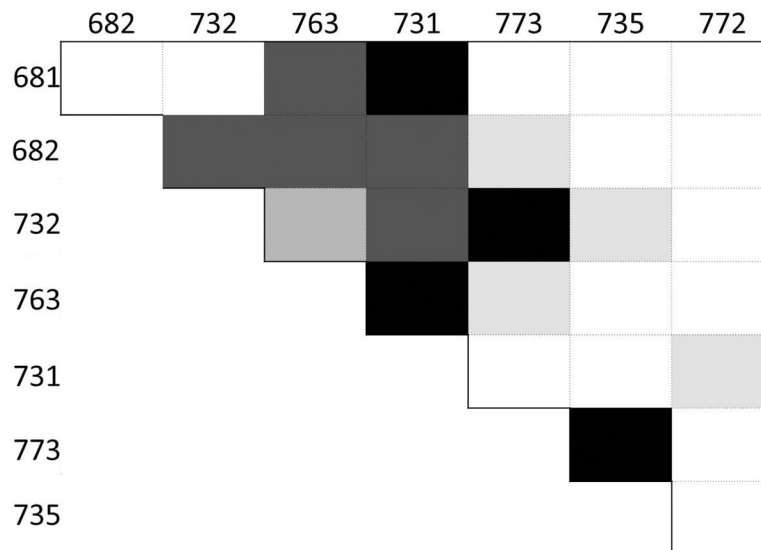
each pair  $(i,j)$  of geckos whether  $i$  is contained in the 95% phenotype cloud of  $j$  or vice versa for each of the two models. If this was not the case for any combination, we assigned a score of 0. If this was the case for one model and in one instance, we assigned a score of 1, etc., up to a maximum possible score of 4. In Fig 11, the maximum score is represented by a black field at position  $(i,j)$ , whereas the minimum score 0 corresponds to a white field, with graded gray levels indicating intermediate scores. The two computational models are largely consistent with respect to their predictions regarding the relatedness of the phenotypes (for example, both models indicate it is highly unlikely that a LALI-type producing a phenotype for #772 would also produce a phenotype for #735). The use of graded gray levels in Fig 11 is a way to summarize where the models were not entirely consistent (all pairs that are not white not black) and present the degree of relatedness by weighting the two models equally.

### Application of the L→P map: Generating the likely variation of an observed phenotype

In Fig 7, Panels C and D, gecko pattern #682 is shown with three patterns that were randomly selected from within the phenotype clouds of each LALI-type, showing the typical random variation for a LALI-type within the neutral region of gecko pattern #682. Within the context of our modeling framework, the variations among these patterns correspond to the random variation of genetic and environmental clones. The patterns shown in Fig 3 (columns 4 and 5) represent the closest phenotype matches generated within each phenotype cloud among 100 simulations for each gecko pattern.

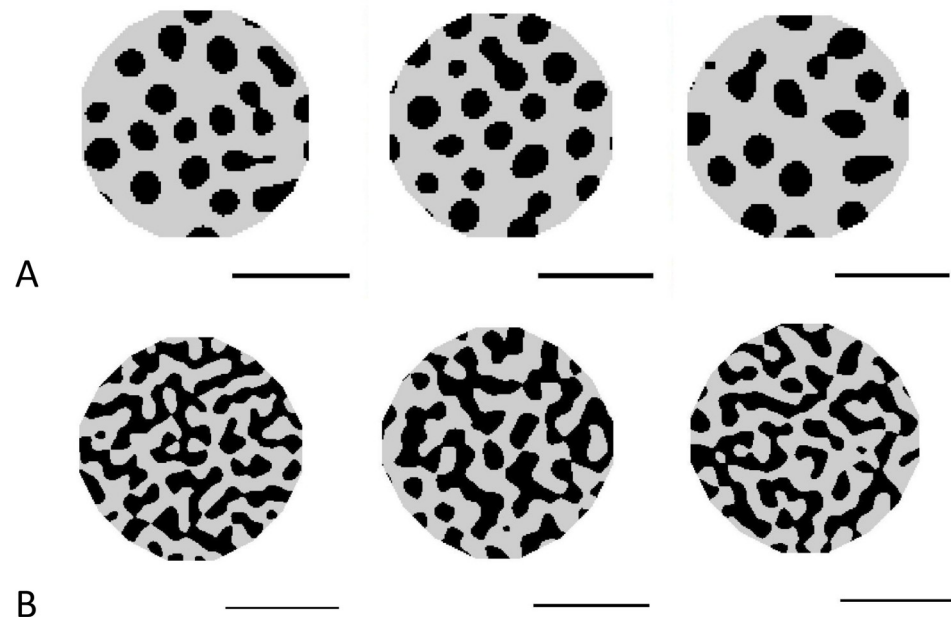
### Application of the L→P map: Generating new patterns outside the likely variation of the group

Just as the  $L \rightarrow P$  map can be used to generate patterns that are within the expected variation of the group, by choosing points in LALI-space just outside the set of neutral regions generated



**Fig 11. Classification of the relatedness of pairs of phenotypes.** Pairs of the geckos IDs 681, 682, 732, 763, 731, 773, 735, 772 are classified according to a measure of relatedness based on the linear and FitzHugh-Nagumo models used in this paper. The main idea of this measure is whether a likely combination of genotype and environmental factors for the head patterning of one of the geckos in a pair can also produce the pattern of the other gecko with developmental noise as the only difference. The darker the color, the closer two patterns are related in this sense, with white color corresponding to the case when neither of the two patterns can be produced by the other’s combination of genetic and environmental factors for any of the models. (See text for the method used to produce the table).

<https://doi.org/10.1371/journal.pcbi.1006943.g011>



**Fig 12. Preternatural' Patterns (Patterns extending beyond the variation observed in the gecko cohort)** The LALI framework can be used to generate patterns that are “nearby” in LALI-space, possibly corresponding to the patterns that could be reached by evolutionary change. For each of the ‘starred’ locations in LALI-space indicated in Fig 8, Panel A, we show three random phenotype variations corresponding to that point in LALI-space. These were generated using the linear Turing model. The  $\mu, T$  LALI-type for the patterns generated in A and B are  $[0.805 \ 1.0]$  and  $[0.835 \ 1.0]$ , respectively. Horizontal bars indicate 0.5 cm.

<https://doi.org/10.1371/journal.pcbi.1006943.g012>

by the group of leopard gecko patterns, we can simulate patterns beyond the expected variation of the group. Fig 12 shows patterns generated from two LALI-types outside the neutral regions of the other eight leopard geckos (the locations of these LALI-types are shown as A and B starred in Fig 8). This corresponds to patterns generated by environmental and genetic parameters outside the range of variability seen within the gecko cohort.

## Discussion

Reptile skin patterning has not been as extensively studied as the skin patterning of mammals (felids, giraffes, zebras) and fish (see Introduction for references). However, reptile integuments also frequently display periodic patterning motifs of stripes, spots and mixed patterns with extensive individual and species variation, furthering the evidence that LALI patterning mechanisms may be widespread among vertebrates. Since coloration and color pattern is achieved very differently in the different groups of vertebrates (e.g., mostly structural, mostly pigment based coloration, or both), knowledge from one group of vertebrates does not necessarily represent what is occurring in other groups and it is worthwhile to investigate apparent similarities. This manuscript adds to studies of reptile integument patterns by describing a set of leopard gecko patterns in the context of LALI patterning.

### Key result: Observed pattern variation of the gecko cohort is more extensive than random variation

In our work, we studied the intra-group variation of patterns selected from a specific region of the head of eight geckos. Considering the variation of the positions of the live gecko patterns

in [FA, EE]-phenotype space (Fig 6), the phenotypes are distributed roughly uniformly in phenotype space, without showing any obvious clusters. A clustering of phenotypes, with a large cluster separation between clusters, would suggest a different genotype-environment contribution for each cluster rather than random variation. Instead, the observed uniform distribution of phenotypes raises the question whether the observed variation of the eight gecko phenotypes may be due to developmental noise alone. In other words, it would be a reasonable hypothesis that the eight studied geckos may all have the same genotype and environment background and that the observed variation is the random variation resulting from self-organized LALI processes (Fig 2).

The LALI-type to Phenotype (L to P) map can quantitatively resolve this question by measuring and then quantitatively comparing the developmental noise that would be predicted for each phenotype. For each of the two LALI models we considered, we found that the resulting phenotype clouds for each of the phenotypes did not all overlap (Fig 10) indicating that developmental noise alone cannot explain the variations among the phenotypes. That is, even though there is much overlap among the phenotype clouds, there is no single-LALI-type that would yield all eight phenotypes by random variation. As shown in Fig 11 where each square corresponds to a pairwise comparison of gecko patterns, the lighter the color of a square, the less likely it is that the two phenotypes are generated by developmental noise alone. For example, a LALI-type producing phenotype #732 with an intermediate fractional area is more likely to also result in a phenotype like #731, with a higher fractional area, or #773, with a lower fractional area, but it would be less likely for a LALI-type producing phenotype #773 to also result in a phenotype like #731 as a result of developmental noise alone.

### Matching of observed patterns and selection of morphometric measurements for matching

For this project, rather than trying to recapitulate the stages of development, for which we do not have many biological details, we use the LALI framework to generate pattern matches for the set of patterns of the gecko at a particular stage in their development (at 9 weeks). Using both of the LALI models we considered in this study, we were able to identify LALI-types that generate quantitatively accurate matches to all eight of the observed spot patterns on the heads of eight geckos (Fig 3), where a ‘match’ was defined as producing patterns with the same fractional area and eccentricity. When parameters are varied, periodic LALI patterns vary with respect to the wavelength of the pattern, the size of peaks relative to the wavelength, and a location along a continuum from discrete peaks (spots) to elongated, contiguous peaks (stripes and spirals). For patterns with spots that are well-separated and discrete, relative peak size to peak separation and the elongation of peaks may be quantified with fractional area and eccentricity, respectively. In this work, we were not interested in comparing absolute size differences among the gecko patterns since gecko growth occurs during patterning, resulting in patterns of different size. Since fractional area and eccentricity are dimensionless numbers, and thus scale-independent, they were a natural set of morphometrics for our LALI patterns.

The pattern match observed in our work suggests that a LALI mechanism, in this case, is sufficient to generate the salient aspects of the variation of the color pattern observed on the head of gecko cohort. It is reasonable to consider that a LALI mechanism would work in tandem with other pattern mechanisms, in which case secondary mechanisms could distort the initial LALI pattern and create patterns that are outside the range of LALI parameters space. For example, a LALI mechanism could establish an initial pattern that is then non-randomly stretched by growth along an oriented direction. However, we were able to match the eight observed gecko patterns by varying LALI parameters.



We defined a pattern match as a matching of fractional area and eccentricity. These are natural morphometric measures for LALI patterns, as described above. Even though we only used two morphometric measurements in our quantitative analysis to generate our best matches, the matches are visually very convincing. However, there were aspects of the patterns that we did not try to match, such as pigment saturation and hue, and the fine-scale texture of the contour of the blotches. These finer details of the pattern would require modeling the development of the gecko pattern (which we did not aim to do here), with biophysical details such as tissue spatial organization and stages of cell differentiation, and knowledge of the relative rates of pattern development versus cell differentiation, which are currently not available to us. On the other hand, there are secondary morphometric measurements, beyond fractional area and eccentricity that could be used to fine tune or further validate pattern matches in the future, such as matching the within-pattern variation of spot sizes, eccentricity etc. While fractional area and eccentricity are aspects of the pattern that we matched in this study, unexpected additional variations among patterns that arise as matches in our results instruct us on salient pattern features and motivate the addition of other morphometric variables for fitting. For example, our objective matching algorithm identified patterns as optimized matches even if they included annuli (pigmented regions with a large interior hole), for example, see two annuli in the FitzHugh-Nagumo match for #773 in Fig 3. These annuli occasionally appeared as a best fit match because the algorithm was optimizing only fractional area and eccentricity. This instructs us that if annuli patterns are unwanted, the topology of the pattern should be added as another parameter to match, to exclude regions of parameter space that generate blotches with empty interiors. Rather than apply that topological constraint now, ad hoc, we leave those patterns with annuli as an example of how an objective algorithm for pattern matching avoids subjective bias in pattern selection (if searching by hand, we might have avoided pattern space with annuli) and thus instructs on the most informative features of patterning. It is also worth considering that some variations of leopard gecko patterns may be found with such annuli.

### The $L \rightarrow P$ maps provides an important metric for interpreting the distances between patterns

The difference in two phenotypes can be quantitatively described by the difference in the morphometric properties of the phenotypes (head size, tail length, average spot size, etc.). The concept of using a LALI model to index the difference between phenotypes is a compelling idea and was recently applied by Ledesma-Duran *et al.* [50]. Ledesma-Duran and co-workers studied how the range of phenotypes (skin pattern) of *Pseudoplatystoma* fishes could be abstractly quantified (indexed) by the variation of one parameter in their reaction diffusion model. The compelling advantage of using a LALI model for indexing is that seemingly complex phenotypic differences in patterns, such as spots versus stripes versus mixed patterns, can be described by a small number of parameters (for example, as observed in [51]).

Whether the pattern variation is measured by absolute morphometric differences or indexed by a mathematical model, the expected random variation of the pattern provides a necessary context for interpreting the measured difference between two patterns. The geometry of the  $L \rightarrow P$  map (that is, how a specific change in LALI-space results in a specific change in phenotype) provides guidance regarding the appropriate way to interpret distance between patterns. For instance, ‘small’ changes in LALI space (due to a combination of genotype and environmental changes) may correspond to large changes in pattern appearances (due to developmental noise). In these cases, the two phenotypes may appear to be very different, when in actuality, they are closely related. The opposite situation may also occur, where two

phenotypes may seem similar, but they would originate from different regions in LALI-space. Our methods help to look beyond morphometric measurements and uncover such ‘hidden’ relatedness.

Further, details of the geometry of the  $L$  to  $P$  mapping may provide clues into the ways that the freedoms and constraints of the developmental mechanism shape the effect of selection pressures on color patterning. The large neutral regions of #735 and #682 indicate that LALI parameters could vary within these regions, with little change in the resulting phenotype, so that parameters could drift in a neutral manner to new regions of LALI-space. Varying sizes of the phenotype clouds indicate that different regions of the  $L \rightarrow P$  map differ in their intrinsic variability. If there is selection for more or less variation, then this may shift the selection pressure from particular phenotypes to particular regions of LALI-space. A rich literature of theory can be applied to such phenotypic landscapes, such as the neutral theory of Kimura [52, 53], survival of the flattest [54] and arrival of the frequent [55].

### Generalizability of this framework for other models of developmental noise

The approach we describe here for generating a metric for the variation of patterning that involves separating the developmental process due to genotype and environmental contribution together versus stochastic sources of phenotype variation (developmental noise) can be applied to any developmental mechanism that permits modeling of pattern generation from a set of fixed initial conditions with stochastic effects.

A local activation long range inhibition (LALI) mechanism is a likely candidate for a patterning mechanism for spot patterning on the heads of a cohort of geckos, especially due to the familiar combination of periodic spots and stripes throughout their body color plan and development, but the molecular details of the mechanism are not known. Rather than commit to a LALI mechanism and yield results that are potentially narrower, we compare two implementations of a LALI core logic: one linear and one non-linear, both reaction diffusion mechanisms. The results of the two LALI implementations are similar overall, especially in the geometry of the maps. This overall similarity can be seen by comparing the relative position and sizes of the neutral regions for each gecko pattern phenotype (Fig 8), the similar direction of the bias of the two maps (Fig 9), and the comparable relative sizes and overlaps of the phenotype clouds (Figs 7 and 10). The commonalities of the  $L \rightarrow P$  maps for these two LALI models will include common properties of LALI maps in general while the more subtle differences between the models (relative size and detailed shape of the phenotype clouds, and the extent of overlap) are differences that can be expected from one LALI mechanism to another. In future work, a broader range of LALI mechanisms might be compared, or it would be interesting to compare the topology of maps generated by more diverse non-LALI mechanisms. This would be especially interesting if differences in the geometry of variation make testable predictions to distinguish competing mechanisms, as suggested by [40] in the context of assessing the effect of parameter perturbations.

### Further applications

Here we describe an approach for taking a very small set of patterns (eight individual gecko patterns were compared in our study) and describing their relative relationship (separation, closeness, potential for overlap) within the context of the LALI framework. Without the underlying LALI framework to describe the random variation, a much larger number of pattern specimens would be needed to define a metric for their variation. That is, when two patterns appear to be similar, measuring the differences between very many patterns would be needed to quantitatively determine whether the difference between these two patterns is relatively

small or large, compared to the average variation observed among the pattern specimens. Within the context of the LALI framework, however, each single pattern specimen can be identified as a region in LALI space (i.e., the set of LALI parameters specific to a given LALI model that is likely to generate this pattern). Once a location has been identified, the LALI model can be interrogated to determine the amount of stochastic variation that can be expected for that location in LALI space (without requiring population statistics).

Here, we select a set of LALI patterns (chosen at a particular simulation time point) that match patterns *in vivo* (at a particular time in development), without considering the time course of those patterns during development. We do in fact mean to put forward a paradigm of creating a library of LALI patterns that can be compared with patterns that occur in nature. A key assumption of this is that LALI-generated patterns have certain features that are inherent to the pattern itself (for example, the variability in the pattern that will be due to noise, or maybe also the topological properties of transitions from one pattern to another) that does not depend on the particular LALI mechanism and/or the developmental history of those patterns over time. This is supported by observations that many mechanisms with the same core LALI logic (molecular, cell-based and/or mechanical) yield similar patterning despite different underlying biological processes [40]. The contexts for which this assumption is valid can be further explored by comparing the features of matching LALI patterns, especially for a broader range of LALI mechanisms.

Within the LALI framework, there is the potential to fruitfully compare the patterns of even a small number of pattern specimens by determining whether their expected ranges of random variation would include one another. There is also the potential for comparisons across species, regardless of differences in the specific underlying LALI mechanism, since patterns are mapped by their morphometric characteristics, not their underlying biophysical parameters. Thus, by mapping species pattern movements in a common LALI space, future investigations may find patterns of variation (for example, long term speciation trends) that are common across species, clades, etc. As we have done here, the LALI framework can be used to determine the fraction of observed diversity that is due to genetic and environment factors, which determines the extent to which specific patterns are inheritable or reproducible. The contribution of developmental noise to pattern diversity can be significant (for example, in [1]) and contribute a selective advantage ('bet-hedging' [56]).

Finally, the LALI framework can be used to explore patterns that are just beyond the space apparently explored by the individual variability, to yield 'supra-natural patterns' that may or may not be represented in the wild. From an evolutionary and ecological point of view, identifying potential color patterns that do not occur in wild animal populations, but that can instead be generated either mathematically or sometimes by targeted captive-breeding efforts, provide a ground to investigate the evolutionary constraints (e.g., selective, genetic or developmental) that impede the occurrence of these phenotypes in nature.

## Conclusions

With image analysis and the selection of several morphometric features for analysis, a difference between two phenotypes can be measured. Without a model of stochastic variation like that of the  $L \rightarrow P$  map, however, it is difficult to interpret the significance of a small difference in phenotypes. The model of variation presented here provides a framework for contextualizing the noisy difference between phenotypes within the context of random variation due to developmental noise. Further, the set of parameters in LALI-space that yields a matching phenotype is an efficient summary of the set of real-world parameters that would be needed to specify that phenotype, for any biological mechanism described with a core LALI logic. This

points to a method for classification and comparison of patterns across a broad range of contexts. This work underscores the need for significant interdisciplinary effort [8] to advance biometric approaches for generating and analyzing phenotype data.

## Supporting information

**S1 Fig. Determination of characteristic Fourier wavelength.** A: a rectangular section of the pattern for Gecko ID #731. B: the corresponding centered Fourier spectrum. Low-frequency components are shown in the center of the image, high-frequency components on the edges. Lighter colors indicate larger values. C: a plot of radially averaged interpolated absolute Fourier coefficient as a function of radius  $\lambda$ . The vertical lines indicate the location of the wavenumber corresponding to the maximum interpolated Fourier coefficient, as well as the interval in which its value is within 90% of the maximum.

(TIFF)

**S2 Fig. Evolution of sample patterns for Gecko #682 and Gecko #772 over 600K simulation time steps for the linear Turing model.** The panels (a-f) show the pattern every 100K time steps for a simulation with parameters corresponding to those of Gecko #682. The LALI-type for Gecko #682 is matched at 200K time steps.

(TIFF)

**S3 Fig. Typical path through phenotype space of patterns over 600K simulation time steps for the linear Turing model.** As the simulation progresses, the morphological properties of the spotted pattern change and create a path through FA-EE phenotype space. The points labeled (a-f), when they appear on the frame, correspond to the panels (a-f) described in [S2 Fig.](#)

(TIFF)

**S4 Fig. Evolution of sample patterns for Gecko #735 and Gecko #773 while the threshold is varied from 80% to 105% of the value used for Gecko #735 for the linear Turing model.**

The panels (a-f) show the pattern every as the threshold varied from 80% to 105% in 5% increments for a simulation with parameters corresponding to those of Gecko #682. The LALI-type for Gecko #682 is matched when the threshold is 100%.

(TIFF)

**S5 Fig. Typical path through phenotype space of sample patterns for Gecko #735 and Gecko #773 while the threshold is varied from 80% to 105% of the baseline values used for Geckos #735 and #773 for the linear Turing model.** As the simulation progresses, the morphological properties of the spotted pattern changes and create a path through FA-EE phenotype space. The points labeled (a-f), when they appear on the frame, correspond to the panels (a-f) described in [S4 Fig.](#)

(TIFF)

## Acknowledgments

We are thankful to Julien Claude and Scott Glaberman for comments on an early version of this manuscript, J. Anderson, E. Brumeier, C. Cummings, M. Detjen, I. Eid, and D. Zarkower for help with gecko care and maintenance and I. Eid for photographing geckos.

## Author Contributions

**Conceptualization:** Maria Kiskowski, Tilmann Glimm, Ylenia Chiari.

**Data curation:** Maria Kiskowski, Tilmann Glimm, Nickolas Moreno, Tony Gamble, Ylenia Chiari.

**Formal analysis:** Maria Kiskowski, Tilmann Glimm, Nickolas Moreno.

**Funding acquisition:** Ylenia Chiari.

**Investigation:** Maria Kiskowski, Tilmann Glimm, Ylenia Chiari.

**Methodology:** Maria Kiskowski, Tilmann Glimm.

**Project administration:** Maria Kiskowski, Ylenia Chiari.

**Resources:** Tony Gamble.

**Software:** Nickolas Moreno.

**Supervision:** Maria Kiskowski, Ylenia Chiari.

**Validation:** Maria Kiskowski, Tilmann Glimm, Ylenia Chiari.

**Visualization:** Maria Kiskowski, Tilmann Glimm, Nickolas Moreno, Tony Gamble.

**Writing – original draft:** Maria Kiskowski, Tilmann Glimm, Ylenia Chiari.

**Writing – review & editing:** Maria Kiskowski, Tilmann Glimm, Nickolas Moreno, Tony Gamble, Ylenia Chiari.

## References

- Gartner K., A third component causing random variability beside environment and genotype. A reason for the limited success of a 30 year long effort to standardize laboratory animals? *Lab Anim*, 1990. 24 (1): p. 71–7. <https://doi.org/10.1258/002367790780890347> PMID: 2406501
- Peaston A.E. and Whitelaw E., Epigenetics and phenotypic variation in mammals. *Mamm Genome*, 2006. 17(5): p. 365–74. <https://doi.org/10.1007/s00335-005-0180-2> PMID: 16688527
- Veitia R.A., Stochasticity or the fatal 'imperfection' of cloning. *J Biosci*, 2005. 30(1): p. 21–30. PMID: 15824438
- Vogt G., Stochastic developmental variation, an epigenetic source of phenotypic diversity with far-reaching biological consequences. *Journal of Biosciences*, 2015. 40(1): p. 159–204. PMID: 25740150
- Ziv N., et al., Resolving the Complex Genetic Basis of Phenotypic Variation and Variability of Cellular Growth. *Genetics*, 2017. 206(3): p. 1645–1657. <https://doi.org/10.1534/genetics.116.195180> PMID: 28495957
- Debat V. and David P., Mapping phenotypes: canalization, plasticity and developmental stability. *Trends in Ecology & Evolution*, 2001. 16(10): p. 555–561.
- Geiler-Samerotte K.A., et al., The details in the distributions: why and how to study phenotypic variability. *Curr Opin Biotechnol*, 2013. 24(4): p. 752–9. <https://doi.org/10.1016/j.copbio.2013.03.010> PMID: 23566377
- Kuhl H.S. and Burghardt T., Animal biometrics: quantifying and detecting phenotypic appearance. *Trends Ecol Evol*, 2013. 28(7): p. 432–41. <https://doi.org/10.1016/j.tree.2013.02.013> PMID: 23537688
- Allen W.L., et al., Why the leopard got its spots: relating pattern development to ecology in felids. *Proc Biol Sci*, 2011. 278(1710): p. 1373–80. <https://doi.org/10.1098/rspb.2010.1734> PMID: 20961899
- Gong Z., et al., Evolution of patterns on *Conus* shells. *Proc Natl Acad Sci U S A*, 2012. 109(5): p. E234–41. <https://doi.org/10.1073/pnas.1119859109> PMID: 22219366
- Willmore K.E. and Hallgrímsson B., CHAPTER 10—Within Individual Variation: Developmental Noise versus Developmental Stability, in *Variation* B. Hallgrímsson and Hall B.K., Editors. 2005, Academic Press: Burlington. p. 191–218.
- Hoekstra H.E., Genetics, development and evolution of adaptive pigmentation in vertebrates. *Heredity (Edinb)*, 2006. 97(3): p. 222–34.
- Hubbard J.K., et al., Vertebrate pigmentation: from underlying genes to adaptive function. *Trends Genet*, 2010. 26(5): p. 231–9. <https://doi.org/10.1016/j.tig.2010.02.002> PMID: 20381892

14. Mills M.G. and Patterson L.B., Not just black and white: pigment pattern development and evolution in vertebrates. *Semin Cell Dev Biol*, 2009. 20(1): p. 72–81. <https://doi.org/10.1016/j.semcdb.2008.11.012> PMID: 19073271
15. Protas M.E. and Patel N.H., Evolution of coloration patterns. *Annu Rev Cell Dev Biol*, 2008. 24: p. 425–46. <https://doi.org/10.1146/annurev.cellbio.24.110707.175302> PMID: 18593352
16. Allen W.L., et al., The evolution and function of pattern diversity in snakes. *Behavioral Ecology*, 2013. 24(5): p. 1237–1250.
17. Rosenblum E.B., Hoekstra H.E., and Nachman M.W., Adaptive reptile color variation and the evolution of the Mc1r gene. *Evolution*, 2004. 58(8): p. 1794–808. PMID: 15446431
18. Summers K. and Clough M.E., The evolution of coloration and toxicity in the poison frog family (Dendrobatidae). *Proc Natl Acad Sci U S A*, 2001. 98(11): p. 6227–32. <https://doi.org/10.1073/pnas.101134898> PMID: 11353830
19. Tibbetts E.A. and Dale J., A socially enforced signal of quality in a paper wasp. *Nature*, 2004. 432(7014): p. 218–22. <https://doi.org/10.1038/nature02949> PMID: 15538369
20. Parichy D.M. and Turner J.M., Temporal and cellular requirements for Fms signaling during zebrafish adult pigment pattern development. *Development*, 2003. 130(5): p. 817–33. PMID: 12538511
21. Murray J.D., *Mathematical biology*. 2nd, corr. ed. Biomathematics. 1993, Berlin; New York: Springer-Verlag. xiv, 767 p.
22. Painter K.J., Maini P.K., and Othmer H.G., Stripe formation in juvenile *Pomacanthus* explained by a generalized Turing mechanism with chemotaxis. *Proc Natl Acad Sci U S A*, 1999. 96(10): p. 5549–54. PMID: 10318921
23. Gierer A. and Meinhardt H., A theory of biological pattern formation. *Kybernetik*, 1972. 12(1): p. 30–9. PMID: 4663624
24. Meinhardt H., Models of biological pattern formation: from elementary steps to the organization of embryonic axes. *Curr Top Dev Biol*, 2008. 81: p. 1–63. [https://doi.org/10.1016/S0070-2153\(07\)81001-5](https://doi.org/10.1016/S0070-2153(07)81001-5) PMID: 18023723
25. Meinhardt H. and Gierer A., Pattern formation by local self-activation and lateral inhibition. *Bioessays*, 2000. 22(8): p. 753–60. [https://doi.org/10.1002/1521-1878\(200008\)22:8<753::AID-BIES9>3.0.CO;2-Z](https://doi.org/10.1002/1521-1878(200008)22:8<753::AID-BIES9>3.0.CO;2-Z) PMID: 10918306
26. Turing A.M., The chemical basis of morphogenesis. 1953. *Bull Math Biol*, 1990. 52(1–2): p. 153–97; discussion 119–52. PMID: 2185858
27. Murray J.D., On pattern formation mechanisms for lepidopteran wing patterns and mammalian coat markings. *Philos Trans R Soc Lond B Biol Sci*, 1981. 295(1078): p. 473–96. <https://doi.org/10.1098/rstb.1981.0155> PMID: 6117906
28. Murray J.D., How the leopard got its spots. *Sci Am*, 1988(258): p. 80–87.
29. Murray J.D., A Pre-pattern formation mechanism for animal coat markings. *Journal of Theoretical Biology*, 1981. 88(1): p. 161–199.
30. Barrio R.A., et al., Modeling the skin pattern of fishes. *Phys Rev E Stat Nonlin Soft Matter Phys*, 2009. 79(3 Pt 1): p. 031908.
31. Painter J., K., *Models for Pigment Pattern Formation in the Skin of Fishes*. 2001.
32. Kondo S. and Asai R., A reaction-diffusion wave on the skin of the marine angelfish *Pomacanthus*. *Nature*, 1995. 376(6543): p. 765–8. PMID: 24547605
33. Maini P.K., et al., Bifurcating spatially heterogeneous solutions in a chemotaxis model for biological pattern generation. *Bull Math Biol*, 1991. 53(5): p. 701–19. PMID: 1933036
34. Murray J.D. and Myerscough M.R., Pigmentation pattern formation on snakes. *J Theor Biol*, 1991. 149(3): p. 339–60. PMID: 2062100
35. Manukyan L., et al., A living mesoscopic cellular automaton made of skin scales. *Nature*, 2017. 544(7649): p. 173–179. <https://doi.org/10.1038/nature22031> PMID: 28406206
36. Landová E., et al., *Ontogenetic switch between alternative antipredatory strategies in the leopard gecko (Eublepharis macularius): Defensive threat versus escape*. Vol. 67. 2013.
37. Minton S.A. Jr A contribution to the herpetology of West Pakistan. *Bulletin of the AMNH*, 1966(134): p. 27–184.
38. De Vosjoli P., et al., *The leopard gecko manual: expert advice for keeping and caring for a healthy leopard gecko*. 2nd edition. ed. 2017, Mount Joy, PA: Fox Chapel Publishing. pages cm.
39. Gamble T., Aherns J., Card V., Tyrosinase activity in the skin of three strains of albino Gecko (*Eublepharis macularius*). *Gekko*, 2006(5): p. 39–44.

40. Hiscock T.W. and Megason S.G., Orientation of Turing-like Patterns by Morphogen Gradients and Tissue Anisotropies. *Cell Syst*, 2015. 1(6): p. 408–416. <https://doi.org/10.1016/j.cels.2015.12.001> PMID: [26771020](https://pubmed.ncbi.nlm.nih.gov/26771020/)
41. Bullara D. and De Decker Y., Pigment cell movement is not required for generation of Turing patterns in zebrafish skin. *Nat Commun*, 2015. 6: p. 6971. <https://doi.org/10.1038/ncomms7971> PMID: [25959141](https://pubmed.ncbi.nlm.nih.gov/25959141/)
42. Murray J.D., *Mathematical biology*. 3rd ed. Interdisciplinary applied mathematics. 2002, New York: Springer.
43. Fitzhugh R., Impulses and Physiological States in Theoretical Models of Nerve Membrane. *Biophys J*, 1961. 1(6): p. 445–66. PMID: [19431309](https://pubmed.ncbi.nlm.nih.gov/19431309/)
44. Nagumo J., Arimoto S., and Yoshizawa S., An Active Pulse Transmission Line Simulating Nerve Axon. *Proceedings of the IRE*, 1962. 50(10): p. 2061–2070.
45. Kondo S. and Miura T., Reaction-diffusion model as a framework for understanding biological pattern formation. *Science*, 2010. 329(5999): p. 1616–20. <https://doi.org/10.1126/science.1179047> PMID: [20929839](https://pubmed.ncbi.nlm.nih.gov/20929839/)
46. Marquez-Lago T.T. and Padilla P., A selection criterion for patterns in reaction-diffusion systems. *Theor Biol Med Model*, 2014. 11: p. 7. <https://doi.org/10.1186/1742-4682-11-7> PMID: [24476200](https://pubmed.ncbi.nlm.nih.gov/24476200/)
47. Ermentrout B., Stripes or spots? Nonlinear effects in bifurcation of reaction—diffusion equations on the square. *Proceedings of the Royal Society of London. Series A: Mathematical and Physical Sciences*, 1991. 434(1891): p. 413.
48. Wang X., Elston R.C., and Zhu X., The Meaning of Interaction. *Human Heredity*, 2011. 70(4): p. 269–277.
49. B., S.J., et al., Why does the magnitude of genotype-by-environment interaction vary? *Ecology and Evolution*. 0(0).
50. Ledesma-Duran A., et al., The interplay between phenotypic and ontogenetic plasticities can be assessed using reaction-diffusion models: The case of *Pseudoplatystoma* fishes. *J Biol Phys*, 2017. 43(2): p. 247–264. <https://doi.org/10.1007/s10867-017-9450-y> PMID: [28567598](https://pubmed.ncbi.nlm.nih.gov/28567598/)
51. Watanabe M. and Kondo S., Is pigment patterning in fish skin determined by the Turing mechanism? *Trends Genet*, 2015. 31(2): p. 88–96. <https://doi.org/10.1016/j.tig.2014.11.005> PMID: [25544713](https://pubmed.ncbi.nlm.nih.gov/25544713/)
52. Kimura M., The neutral theory of molecular evolution. *Sci Am*, 1979. 241(5): p. 98–100, 102, 108 passim. PMID: [504979](https://pubmed.ncbi.nlm.nih.gov/504979/)
53. Zhang J., Neutral theory and phenotypic evolution. *Mol Biol Evol*, 2018.
54. Wilke C.O., et al., Evolution of digital organisms at high mutation rates leads to survival of the flattest. *Nature*, 2001. 412(6844): p. 331–3. <https://doi.org/10.1038/35085569> PMID: [11460163](https://pubmed.ncbi.nlm.nih.gov/11460163/)
55. Schaper S. and Louis A.A., The arrival of the frequent: how bias in genotype-phenotype maps can steer populations to local optima. *PLoS One*, 2014. 9(2): p. e86635. <https://doi.org/10.1371/journal.pone.0086635> PMID: [24505262](https://pubmed.ncbi.nlm.nih.gov/24505262/)
56. Nichol D., et al., Stochasticity in the Genotype-Phenotype Map: Implications for the Robustness and Persistence of Bet-Hedging. *Genetics*, 2016. 204(4): p. 1523–1539. <https://doi.org/10.1534/genetics.116.193474> PMID: [27770034](https://pubmed.ncbi.nlm.nih.gov/27770034/)
57. Gillespie D.T. A general method for numerically simulating the stochastic time evolution of coupled chemical reactions. *Journal of Computational Physics*, 1976. 22, p. 403–434.
58. Woolley T.E., Baker R.E., Gaffney E.A., Maini P.K., Seirin-Lee S., Effects of intrinsic stochasticity on delayed reaction-diffusion patterning systems. *Phys. Rev. E*, 2012. 85,
59. Kaern M., Elston T.C., Blake W.J., Collins J.J., Stochasticity in gene expression: from theories to phenotypes. *Nat. Rev. Genet*. 2005. 6, 451–464. <https://doi.org/10.1038/nrg1615> PMID: [15883588](https://pubmed.ncbi.nlm.nih.gov/15883588/)
60. Climescu-Haulica A., Quirk M.D., A stochastic differential equation model for transcriptional regulatory networks. *BMC Bioinformatics* 2007. 8, S4.